Circuit type simulations of magneto-transport in the quantum Hall effect regime

2006 J. Phys.: Condens. Matter 18 R101

(http://iopscience.iop.org/0953-8984/18/7/R01)

INSTITUTE OF PHYSICS PUBLISHING JOURNAL OF PHYSICS: CONDENSED MATTER

J. Phys.: Condens. Matter **18** (2006) R101–R138 doi:10.1088/0953-8984/18/7/R01

TOPICAL REVIEW

Circuit type simulations of magneto-transport in the quantum Hall effect regime

Josef Oswald and Manfred Oswald

Institute of Physics, University of Leoben, Franz Josef Strasse 18, A-8700 Leoben, Austria

E-mail: josef.oswald@unileoben.ac.at

Received 23 September 2005, in final form 5 January 2006
Published 30 January 2006
Online at stacks.iop.org/JPhysCM/18/R101

Abstract

Localization in the bulk is one of the most important ingredients for the theory of the quantum Hall effect and much attention has been paid to this topic for more than two decades. However, less effort has been made to model the current transport itself. Network models are frequently used in this context and an answer should be given as to whether these are also suitable for modelling the lateral distribution of experimentally excited currents and voltages in the quantum Hall effect (QHE) regime. The term 'network model' is of more general meaning and therefore the term 'circuit type simulations' should be used instead for expressing this kind of modelling. In preceding papers a Landauer–Büttiker type representation of bulk current transport has been successfully used for the numerical simulation of the magneto-transport of two-dimensional electron systems in the high magnetic field regime. This approach allows us to build up a network model, which describes correctly the effect of non-equilibrium currents injected via metallic contacts as in real experiments. In this context we suggest a network model, which serves as a circuit type representation of magneto-transport. It is demonstrated that it is in full agreement with a treatment of bulk current transport as a quantum tunnelling process between magnetic bound states, which exist in the high magnetic field regime. Additionally, we find a striking correspondence between our network representation and the bulk current picture in terms of mixed phases mapped on a chequerboard: at half filled Landau level (LL) coupled droplets of a quantum Hall (QH) liquid phase and coupled droplets of an insulator phase exist at the same time, with each of them occupying half of the bulk area. Removing a single electron from such a QH liquid droplet at half filling completes the QH plateau transition to the next higher QH plateau, while adding a single electron to such a droplet at half filling completes the QH plateau transition to the previous lower QH plateau. As a consequence, the sharpness of the QH plateau transitions on the magnetic field axis depends on the typical size of the droplets, which can be understood as a measure of the disorder in the sample. We furthermore demonstrate that our model can also be used as a

theoretical concept for discretization of a long range random potential on a regular grid. We also find a correspondence between our model and the so called localization picture of the QH plateau transitions. Alternative approaches like the Chalker–Coddington (CC) network as the coherent counterpart and a resistor network as the classical counterpart are discussed in comparison with our network approach. On the one hand the CC model was originally developed to treat the localization problem; on the other hand it also assigns currents to channels, and in this context the CC model will be discussed in the context of circuit type simulations as well. Finally, we compare our simulation results to results obtained on the basis of an adapted lattice model by Ando (1998 *Surf. Sci.* **361/362** 270) for the QHE regime and find our results in full agreement for the case of strong inelastic scattering.

(Some figures in this article are in colour only in the electronic version)

Contents

1. Introduction

Even more than 20 years after the discovery of the integer quantum Hall effect there are still controversial discussions about the origin of this phenomenon. In particular, the transition regime between plateaus has gained increasing attention during the last two decades. While it is commonly accepted that the plateau values of the integer quantum Hall effect (IQHE) can be explained by the edge channel (EC) picture of the IQHE [1–4], the transition regime between plateaus is believed to be driven by a different mechanism in the bulk of the sample. A well defined scaling behaviour of the temperature dependence is seen as evidence for a quantum phase transition in the vicinity of the QHE plateau transitions [5–9] (for a review see also [10, 11]). While the existence of a formal equivalence of the EC picture and the bulk current picture is proposed by Ruzin *et al* [12], the investigations of non-equilibrium situations like selective EC population, AC characteristics and non-linear transport give evidence that ECs are more than just a different representation of bulk current transport. For more than two decades the fundamental question concerning edge versus bulk in the QHE has received permanent attention, even until now, as can be seen from a representative selection of references. As a starting point we consider the discovery of the IQHE [13] and first systematic experiments investigating different contact configurations [14, 15], going on with a systematic

theoretical approach making use of the Landauer formula in the context of ECs [1, 16, 17], which finally resulted in the so called Landauer–Büttiker formalism. There exist already an enormous number of examples for dealing with the edge versus bulk problem and making use of the EC picture for modelling and interpretation of experiments [18–92]. But also a remarkable number of most recent papers on this topic can be found [93–113]. Concerning experimental probing of ECs, major improvements of the experimental techniques have been achieved in the last few years [37, 44, 48, 52, 78, 80–83, 88, 89, 111]. A very fundamental aspect of ECs is the drastic enhancement of the phase coherence length of electrons in edge states and major work on this topic has been done by Komiyama *et al* [94]. Concerning modelling of quantum transport, one of the very first attempts can be attributed to Landauer [114, 115], who introduced the so called Landauer formula for current transport in 1D channels. The existence of current carrying edge states was first proposed by Halperin [116], and one of the most prominent representatives of the ongoing work is Büttiker, who developed and established the so called Landauer–Büttiker (LB) formalism and made the EC picture of the IQHE [1] popular and applicable for the scientific community. As early as 1987 Streda *et al* [16] considered the Landauer formula for an abstract scattering region connected by ideal leads, which the authors proposed to be well suited for explaining QHE experiments in narrow channels. About the same time Jain *et al* [17] aimed at the modelling of the QHE in narrow channels. They proposed resonant tunnelling across a magnetic bound state as the mechanism for experimentally observed resistance fluctuations in narrow QHE samples. Magnetic bound states are also a major ingredient of our network model, as outlined in more detail below. For modelling quantum transport and localization in the bulk, mainly network models based on the Chalker–Coddington (CC) network [117] are used. However, a network model which generates data in terms of voltages and resistances, which would allow a direct comparison with experimental data for realistically shaped samples, had not been developed on the basis of the CC model. Some time ago, we made an approach to combine EC transport and bulk transport [68, 71]. Subsequently, that model was expanded to a network [85], which is also a main subject of this paper. In contrast to a CC network our network does not use a transfer matrix for amplitudes and phases. We use transmission by tunnelling, but incorporating the effect of tunnelling according to the LB formalism. The nodes are described by a backscattering function P, which corresponds to the ratio of reflection and transmission coefficient R/T in the LB formalism. Another major difference is that the CC network deals with the (persistent) equilibrium currents of the directed channels and magnetic bound states, while our network deals exclusively with non-equilibrium currents and potentials. Since in transport experiments only non-equilibrium currents are monitored, our network approach is applicable to model directly experimental data.

2. Different types of models

Before introducing different types of models and their comparison, we want to present the main motivation, which can be considered as common for all these approaches. From this it will be easier to catch the main goals of the different approaches which turn out to go in substantially different directions. As already mentioned in the introduction, the main motivation of all models is the theoretical explanation of the IQHE, discovered by Klitzing. The typical appearance is as follows. Close to integer filling factors the Hall voltage shows plateaus while varying either the perpendicular magnetic field B at fixed carrier density or varying the carrier density via a gate electrode at fixed magnetic field. The latter was the original experimental configuration used by Klitzing when discovering the QHE, but the commonly known and most frequently used configuration is the first one. While the Hall voltage shows plateaus the longitudinal voltage vanishes, indicating dissipation-less transport along the sample.

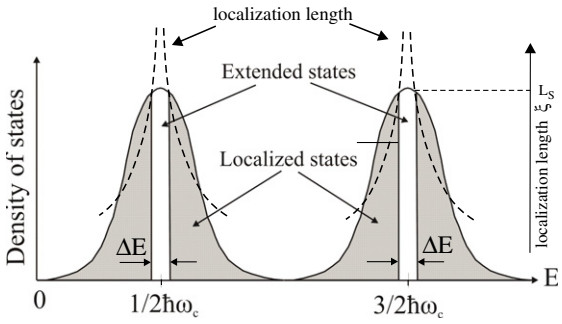

Figure 1. Schematic representation of the density of states (bold curves) of the LLs and the energy dependence of the localization length (dashed curves). Close to the centre of the LLs the localization length diverges for one particular energy. At finite sample size L_S all states of localization length larger than the sample size L_S appear to be de-localized (non-shaded area around the LL centre) while all states in the tails of the LLs appear to be localized (shaded areas). ΔE is the energy interval of the de-localized states.

The commonly accepted picture of the QH regime is that the 2D sub-bands are split by LLs, which get broadened due to inhomogeneities and potential fluctuations. The DOS of the LLs close to the LL-centre consists of de-localized states, while the DOS in the tails of the LLs consists of localized states, which do not contribute to current transport, but are important for the pinning of the Fermi level in the plateau regime of the QHE (see figure 1). If the Fermi level lies within the localized states of the bulk region, de-localized states appear at the Fermi level only at intersections of the Fermi level with the LLs close to the sample edge. This is because the LLs get bent up at the sample edge due to the work function of the host material. These intersections form directed channels (ECs) and each pair of such ECs contributes exactly the universal conductance e^2/h to the total conductance of the system (see figure 2). The two-terminal voltage U in this regime appears at the same time as the Hall voltage U_H and determines the longitudinal sample current according to $I = GU$ and $G = \jmath e^2/h$, with $\jmath$ the number of EC pairs. This leads finally to the two-terminal resistance $R = (1/j)(h/e^2)$, which is at the same time the quantized Hall resistance R_H. j is the integer part of the LL filling factor ν. The situation becomes more complicated if the Fermi level enters the regime of de-localized states. In this regime bulk and edge currents appear in parallel and the bulk current serves as a backscattering process between opposite ECs, which also brings up dissipation. Therefore, the Hall resistance departs from the plateau value and a longitudinal voltage drop appears. If this happens while e.g. sweeping up the magnetic field, the Fermi level crosses the de-localized states of the top LL and it finally enters the localized states of the low energy tail, making the bulk insulating again. However, during this process one pair of ECs gets lost, leading to the next higher plateau of the quantized Hall resistance. As a consequence, a QH plateau transition is performed while the Fermi level crosses the region of the de-localized states, thus suggesting the QH plateau transition to be an effect which is driven by a localization–de-localization mechanism of the bulk states.

Much effort has been made to find the proper function for the localization length versus energy $\xi(E)$, where E is the energy of the considered state. All analytical and numerical results so far are consistent with the picture that at absolute zero temperature the localization length diverges for one specific energy E_c close to the LL centre with a universal exponent γ according to

$$\xi(E - E_c) = \frac{\xi_n}{|E - E_c|^\gamma}. \tag{1}$$

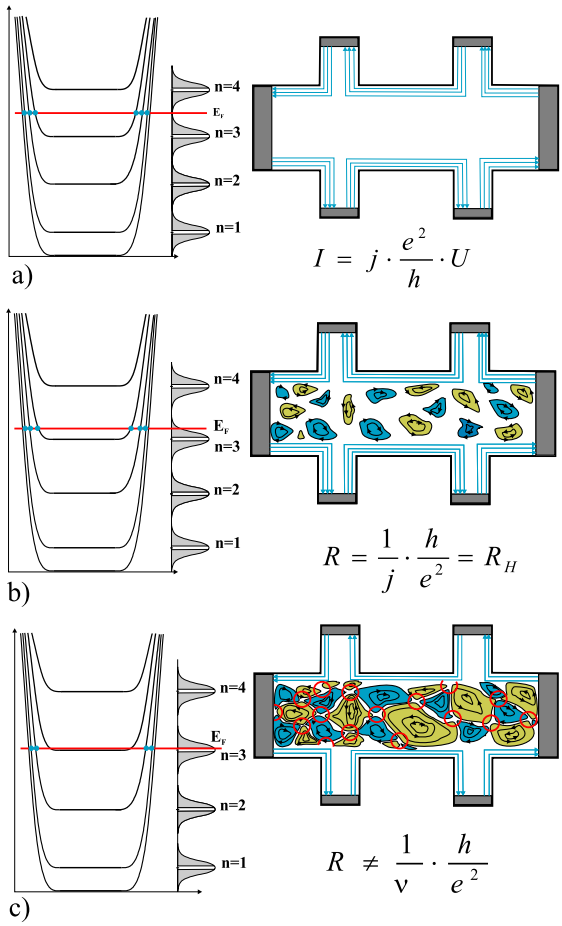

Figure 2. Schematic representation of the formation of edge channels. The left column (a)–(c) shows the lateral variation of the LLs in a cross cut of a Hall bar at different positions of the Fermi level (the broadened LLs on the right of the diagram are indicated for the bulk region and correspond to figure 1). The right column (a)–(c) shows the Hall bar geometry together with the corresponding lateral extension of the intersections between LLs and Fermi level. As long as the Fermi level lies within the localized states (case (a), (b)), the whole sample current is carried by pairs of edge channels and the Hall resistance R shows a plateau value, just depending on the number j of involved EC pairs (number of fully occupied LLs). The bulk builds disconnected localized magnetic bound states (closed de-coupled edge channel loops). The two-terminal resistance R in this case coincides exactly with the Hall resistance R_{H}. Case (a) is an idealized situation, which is unlikely for real systems because of insufficient pinning of the Fermi level due to missing bulk states. If the Fermi level lies within the de-localized states close to the LL centre, edge and bulk current appear in parallel, which destroys the Hall plateau. In this case the bulk states couple at the saddles (see encircled regions on the right in case (c)) of the random potential and thus allow bulk current flow.

For a review see [10]; a most recent review can also be found in [123]. The boundary between localized and de-localized states within a LL determines the width of the associated plateau transition regime, which has been investigated experimentally as well [5–9, 124]. As already mentioned, for a sample of infinite size at absolute zero temperature, this transition regime is expected to shrink to zero since an infinite localization length is expected only at one certain energy E_{c} close to the LL centre. At finite sample size the transition regime

widens since all states localized on a length larger than the sample size L_S appear as de-localized and contribute to transport. But this is not the only effect which widens the transition regime. Another possibility is a finite temperature, as present in experiments. This temperature dependence has been widely investigated, known as the temperature scaling of the QHE plateau transitions. Qualitatively this effect can be understood in terms of a phase uncertainty, which is brought in by the temperature and which becomes most pronounced in quantum interference effects taking place over long distances. Therefore, a localization mechanism based on quantum interference, such as e.g. Anderson localization, breaks down for a localization lengths larger than a critical temperature dependent length $L_T \propto T^{-p/2}$, with p being a non-universal exponent. This means that a finite temperature leads to a de-localization of all states which have a localization length larger than L_T at zero temperature. If now L_T becomes smaller than the sample size, the plateau transition regime widens with increasing temperature. This manifests in a power law scaling of the plateau transition width on the magnetic field axis like $\Delta B \propto T^{\kappa}$. However, for a given system, ΔB corresponds directly to the energy interval of de-localized states ΔE. This allows us to link the temperature scaling function with the function for the localization length ($\Delta B \propto T^{\kappa} \propto \Delta E \propto L_T^{-1/\gamma} \propto T^{p/2\gamma}$), which couples the universal exponent γ with the temperature scaling exponent κ like $\kappa = p/2\gamma$ [125]. The appearance of the additional parameter p makes it difficult to use temperature scaling exclusively as a tool to prove the universal exponent γ experimentally and also tells us that the temperature scaling exponent κ may not be universal as well. Therefore other types of scaling experiments had to be used as well, such as e.g. size scaling, frequency scaling, current scaling and others (see e.g. [124] and references therein). However, since the scaling theory is not the topic of this paper, we would like to refer to the cited literature for further details at this point. But the introduction given so far should be sufficient to make clear that the theory of localization in the QHE regime has to be one major topic in the theory of the QHE.

If considering different theoretical approaches, one has to distinguish the goals of the different approaches at first. The CC model, which will be summarized in the next sub-section, is aimed at modelling the localization length at different energies, as addressed above, but not modelling the current transport itself. In contrast, our model, which we are going to introduce afterwards, aims directly at modelling the current transport and all related phenomena in various QH experiments with different sample geometries. Although not really belonging to the family of network models, the lattice model, as e.g. used by Ando *et al*, is introduced briefly as a third possible approach. The lattice model was originally also dedicated to calculating the localization length like the CC model. However, it brings up interesting new aspects in the context of in-elastic scattering and dissipation, which turn out to be quite important for the discussion of the network models as well. On the one hand our proposed network model seems to be based on the same theoretical background as the CC model, but on the other hand it is substantially different from the CC model in handling the coupling at the nodes. Therefore, in another separate sub-section, special attention is paid to the ability of the CC model to also model experimentally excited currents and voltages, in comparison to our proposed model. Another sub-section is dedicated to a discussion of our network approach in terms of a resistor network as the classical counterpart of the CC model, which at the same time concludes section 2.

2.1. The Chalker–Coddington network model

As already mentioned above, the original goal of the Chalker–Coddington (CC) concept was to calculate the localization length of the electronic states in the high magnetic field limit as a function of energy. The basic idea behind is to consider Anderson localization, which in general would require to solve Schrödinger's equation for obtaining the electronic states. In this context

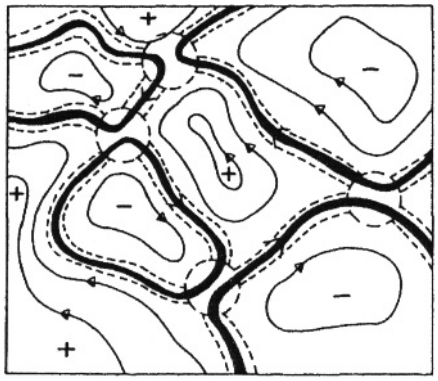

Figure 3. Schematic lateral potential distribution after [117]. The full curves represent equipotentials and the arrows give the direction of transmission. The + and − denote maxima and minima. The bold line represents the contour along which the electronic state is extended. The perpendicular extension is indicated by the broken curves. The broken circles mark the coupling regions, which become the nodes of the network.

the CC model is a powerful method to circumvent a direct solution of Schrödinger's equation by considering mainly the following facts: (a) the electronic states exhibit unidirectional transmission (directed channels) and (b) the extension of the wavefunction follows almost exactly the equipotential lines of the random potential, while it is localized on the length scale of the magnetic length perpendicular to the equipotential lines. Following [117], this is schematically shown in figure 3. Applying the current density operator to such expected electronic states, one has to demand current conservation all along the channels between the nodes. These nodes are formed by the saddles of the random potential (encircled regions in figure 3). Another important ingredient is current conservation at the nodes itself, which requests a unitary matrix between the transmitted amplitudes of incoming and outgoing channels. Since the associated currents correspond to transmitted wavefunction amplitudes by the directed channels, the only degree of freedom along the channels outside the nodes is left for the phase.

Figure 4 shows schematically the trajectories of the channels while passing a saddle point or being reflected at the saddle point of the potential. The transmitted amplitudes of the wavefunctions across the saddles are associated with currents and the current conservation of incoming and outgoing channels demands [117, 123]

$$|\psi_1|^2 + |\psi_3|^2 = |\psi_2|^2 + |\psi_4|^2. \tag{2}$$

This is maintained by the unitary scattering matrix S:

$$\begin{pmatrix} \psi_2 \\ \psi_4 \end{pmatrix} = S \begin{pmatrix} \psi_1 \\ \psi_3 \end{pmatrix}. \tag{3}$$

S has the general form

$$S = \begin{pmatrix} \mathrm{e}^{-\mathrm{i}\varphi_2} & 0 \\ 0 & \mathrm{e}^{\mathrm{i}\varphi_4} \end{pmatrix} \begin{pmatrix} -r & t \\ t & r \end{pmatrix} \begin{pmatrix} \mathrm{e}^{\mathrm{i}\varphi_1} & 0 \\ 0 & \mathrm{e}^{-\mathrm{i}\varphi_3} \end{pmatrix} \tag{4}$$

with r the reflection and t the transmission coefficient for the amplitudes. An equivalent representation is the usage of the so-called transfer matrix T:

$$\begin{pmatrix} \psi_4 \\ \psi_3 \end{pmatrix} = T \begin{pmatrix} \psi_1 \\ \psi_2 \end{pmatrix} \tag{5}$$

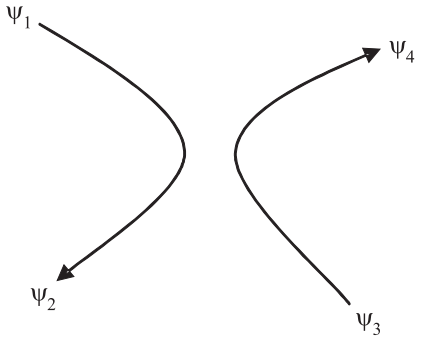

Figure 4. Node of the network with two incoming and two outgoing channels. The channels in the Chalker–Coddington network are treated according to the transfer matrix, which relates transmitted amplitudes and phases of the wavefunctions on the left (ψ_1, ψ_2) to the transmitted amplitudes and phases of the wavefunctions on the right (ψ_3, ψ_4).

with

$$T = \begin{pmatrix} e^{i\varphi_4} & 0 \\ 0 & e^{i\varphi_3} \end{pmatrix} \begin{pmatrix} 1/t & r/t \\ r/t & 1/t \end{pmatrix} \begin{pmatrix} e^{i\varphi_1} & 0 \\ 0 & e^{i\varphi_2} \end{pmatrix} \tag{6}$$

where current conservation requires

$$J = T^{\dagger} J T \tag{7}$$

with

$$J = \begin{pmatrix} 1 & 0 \\ 0 & -1 \end{pmatrix}. \tag{8}$$

Due to current conservation ($t = \sqrt{1 - r^2}$), the transfer matrix T can be described by a single parameter Θ, with Θ and φ real [117]:

$$T = \begin{pmatrix} e^{i\varphi_4} & 0 \\ 0 & e^{i\varphi_3} \end{pmatrix} \begin{pmatrix} \cosh\Theta & \sinh\Theta \\ \sinh\Theta & \cosh\Theta \end{pmatrix} \begin{pmatrix} e^{i\varphi_1} & 0 \\ 0 & e^{i\varphi_2} \end{pmatrix}. \tag{9}$$

Here $E \gg E_C$ (E_C being a critical energy near the centre of the LL and E the energy of the transmitting state) corresponds to $\Theta \ll 1$ and $E \ll E_C$ corresponds to $\Theta \gg 1$ [117]. Against this background Θ is a monotonic function of the energy with respect to the critical energy near the LL centre and is considered to depend linearly on the energy close to the LL centre. A change between the cases $\Theta \ll 1$ and $\Theta \gg 1$ corresponds to a switching from either full transmission to full reflection or vice versa, which at the same time acts like a rotation of the node by 90°. This can also be seen from figure 6, when shifting the Fermi level from the low energy tail to the high energy tail of the LL. Realistically, one should study a network that is topologically disordered; instead, it has been supposed that randomness in the link phases of the channels which connect the nodes is sufficient while using a square lattice. For calculating the localization length, long narrow samples have been built on the basis of this network, which are connected to infinitely long ideal conductors on both sides. Periodic boundary conditions have been applied across the width of the sample, which thus represents a cylinder geometry. Figure 5 shows the network layout as used in [117].

The main purpose was to calculate the transfer matrix of the whole network, which relates the amplitudes on the left to those on the right. The network has been cut into slices with the total transfer matrix being the product of the transfer matrix of each of the slices. For the high energy tail ($\Theta \ll 1$) and low energy tail ($\Theta \gg 1$) the above network reduces to situations like

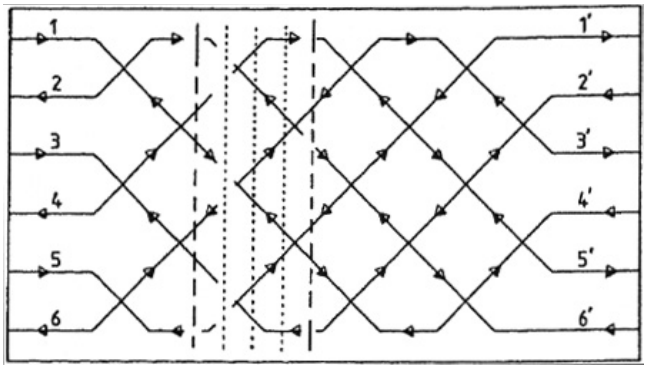

Figure 5. The CC network of [117] with strip boundary conditions, connected to semi-infinite ideal conductors. A 'slice' of the network is defined between dashed vertical lines and each slice is divided into four different sub-slices, divided by the dotted lines. Each sub-slice is represented by a transfer matrix and their product gives the transfer matrix of a whole slice. The transmission through the whole system then is the product of all slices.

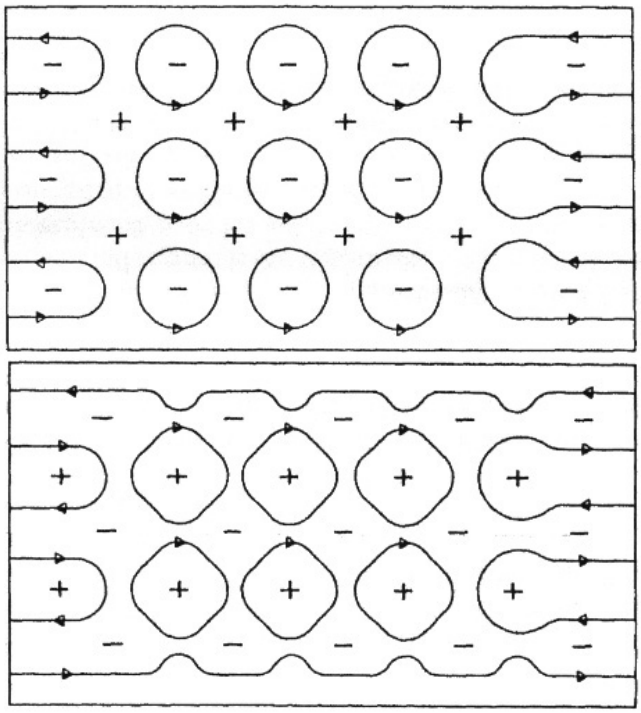

Figure 6. The network of figure 5 reduces to a set of disconnected loops (upper part) if the Fermi level enters the low energy tail of the LL, while disconnected loops coexist with a freely percolating channel (lower part) if the Fermi level lies within the high energy tail of the LL. This matches the behaviour also sketched in figure 2.

those sketched in figure 6. Without going into further details, CC have been able to show that except for one value of $\Theta_c = 0.8814$ all states tend to be localized. CC finally managed to fit the power law dependence of the localization length versus $\Theta - \Theta_c$ and obtained a slope of

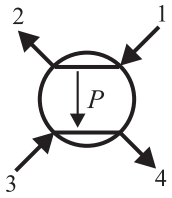

Figure 7. Node of the network with two incoming and two outgoing channels. The channels $1 \rightarrow 2$ and $3 \rightarrow 4$ are treated like ECs with backscattering, where $P = R/T$ according to the Landauer–Büttiker formalism.

$\gamma = 2.5$, which corresponds to the exponent of the localization already mentioned above in equation (1). For the ongoing discussion later on in this paper, further details of the CC model and the transfer matrix approach are not needed. Quite a number of variations and extensions of the CC model have been made by different authors, all of them using the transfer matrix approach. As a consequence, all conclusions drawn from the usage of such a transfer matrix also apply to these models. A most recent extensive review of random network models is given by Kramer *et al* [123]. The authors therefore refer to the literature for further details. The main facts presented so far will be picked up again in another sub-section in the context of the question about the possibility of circuit type simulations on the basis of the CC network model.

2.2. Our proposed network model

The basic layout of our proposed network looks similar to the above introduced and often used CC network (see figures 3–6). However, the CC network has been set up as a method to calculate the localization length in the QH regime, while our model aims directly at modelling the transport of experimentally excited currents. Therefore, the handling of the nodes as well as the association of the channels with currents and potentials is substantially different. This is considered in more detail in the following.

In figure 7 a single node of our network is shown, which transmits potentials from the incoming to the outgoing channels. This figure can be associated with figure 4, but the transmitted potentials of the outgoing channels as a function of the potentials of the incoming channels is calculated as follows [85]:

$$u_2 = (u_1 + Pu_3)/(1 + P) \tag{10a}$$

$$u_4 = (u_3 + Pu_1)/(1 + P). \tag{10b}$$

It is most important to note that, in contrast to the CC network, in our network currents are attributed to channel pairs while in the CC model the currents are attributed to the individual single directed channels. As an example, in our case the longitudinal current I from the right to the left is described by $I = (e^2/h)(u_1 - u_4) = (e^2/h)(u_2 - u_3)$. However, the other possibility to build a pair of channels describes a current $I_R = (e^2/h)(u_1 - u_2) = (e^2/h)(u_4 - u_3)$, which is a transverse or backscattering current between the channel pairs (indicated by the arrow for scattering in figure 7). The ratio of I/I_R corresponds to the relation of the transmission and reflection coefficients R/T of the Landauer–Büttiker (LB) formalism and has been given the symbol P in our model. It allows us to set up the above equations, which describe the potentials u_2 and u_4 of the outgoing channels as a function of the potentials of the incoming channels u_1 and u_3. These equations incorporate current conservation for both I and I_R separately. It is interesting to note already at this point that in this way our nodes of the network provide a handle to potentials as well as to currents, as one has to expect

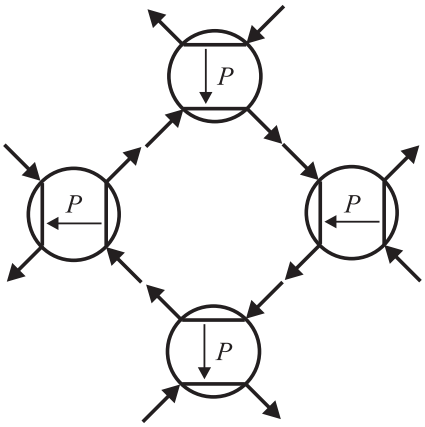

Figure 8. Arrangement of the nodes for building the minimal physical element of a network, which is the closed loop of a so-called magnetic bound state (see the text).

from a circuit-type network model (in contrast to the CC model, see below). The physical background of P will be investigated theoretically in more detail in section 3 of this paper. In figure 8 it is shown how our network is built by arranging the nodes. The minimum network forms a loop, which corresponds physically to a single magnetic bound state. A periodic continuation of this network leads to further adjacent loops, which get coupled by the nodes. In this way the network transmits potentials and the potential distribution is calculated by an appropriate iteration procedure. Currents are calculated only after obtaining the solution for the potential distribution within the whole network. Because of using just reflection and transmission coefficients so far, phase coherence between adjacent loops is not explicitly included. Against this background it is quite remarkable that our network allows us to simulate IQHE experiments with realistic sample geometry in agreement with experimental data in almost all details [85, 90, 113]. Considering the nodes of the network, they can be understood as interconnected elementary QH samples with a single EC pair experiencing backscattering. This backscattering is described by the function P. Originally P was used as representative for a QHE sample as a whole and it is defined for each LL separately as a function of the filling factor $P = P(\Delta\nu)$ [68, 71]. $\Delta\nu$ is the filling factor of the corresponding LL relative to half filling. The total sample behaviour is obtained by summing up the components of the conductance tensor of all LLs. In [71] it was shown that in order to meet all symmetry relations found in experimental data [62, 67] $P(\Delta\nu)$ has to be an exponential function $P(\Delta\nu) = \exp(-\Delta\nu/k)$ with k being a parameter responsible for the sharpness of the plateau transitions. Against this background this function has to be seen as a semi-empirical function so far. Nevertheless, just assuming the existence of this function allows us to explain already quite a number of universal features of the IQHE without referring to a special choice of the pre-factor k in the exponent. The function $P(\Delta\nu)$ also allows us to obtain a scaling behaviour by considering the factor k as a temperature dependent function $k(T)$. In [71] it has been shown that any not necessarily known function $k(T)$ is mapped out directly by the temperature scaling function for R_{xx} and R_{xy}. The basic idea, which subsequently led to the usage of $P(\Delta\nu)$ also within a network approach, is that current transport at high magnetic fields in the bulk region may happen via tunnelling between magnetic bound states. Such bound states are considered to be physically equivalent to ECs. Thus, these bound states are closed loops of directed channels and are created in real samples by smooth potential fluctuations at high magnetic fields. Tunnelling between such

loops happens preferably near the saddle points of the random potential, as considered by the CC model as well. Based on this, our network model is a model of non-interacting carriers occupying magnetic bound states. However, this does not necessarily mean that our model might not be also applicable to a regime of strong interactions, provided that the interactions are incorporated in a model of non-interacting quasi-particles, like the composite fermions. However, this will be the topic of future work. The most important element of our network is that the tunnelling current can be handled as a backscattering process in the EC picture as already mentioned above. This makes our network approach essentially different from the CC model [117] and all network approaches derived from this [120–123]. Just to clarify, the CC network maintains coherence on the entire network, while the largest coherent element in our network is a single loop, which at the same time defines the size of a network period L. If we consider the inelastic scattering length L_{in} of the electron system and the size of the sample L_{S}, then the CC network deals with the regime $L < L_{\mathrm{S}} \leqslant L_{\mathrm{in}}$, while our network considers the regime $L_{\mathrm{in}} \leqslant L < L_{\mathrm{S}}$. From this point of view our network does not necessarily contradict the CC network, but it addresses a different regime. Because $L_{\mathrm{in}} \leqslant L < L_{\mathrm{S}}$ the possibility of dissipation within the nodes of the network must also be incorporated in the formal description. In order to be precise we point out that the nodes have to account for a possible presence of dissipation without necessarily describing the real microscopic scattering mechanism. The longitudinal voltage drop due to backscattering already implies the presence of dissipation, which is briefly considered in the following. Referring to figure 7, the longitudinal voltage drop is given by

$$u_1 - u_2 = P(u_1 - u_4). \tag{11}$$

The longitudinal current I is

$$I = \frac{e^2}{h}(u_1 - u_4). \tag{12}$$

On this basis the dissipated power $p = I(u_1 - u_2)$ can be written as

$$p = P\frac{e^2}{h}(u_1 - u_4)^2. \tag{13}$$

As a consistency check we look also for an alternative view of the backscattering process. This is achieved by associating the backscattering process itself directly with the tunnelling current I_{R}. I_{R} is related with the longitudinal current I by $I_{\mathrm{R}} = PI$ and consequently the associated dissipated power p can be re-written as follows: $p = I_{\mathrm{R}}(u_1 - u_4)$, which finally can be transformed back to equation (13). This demonstrates that on the one hand the involved potentials and currents are able to represent dissipation and on the other hand the involved equations, which couple the different currents and potentials, are in agreement with energy conservation. At this point it is interesting to note that Ando *et al* [119], who aimed at modelling the lateral potential distribution in the plateau transition regime, needed to introduce artificial metallic point contacts as thermal reservoirs. These have been distributed all over the bulk area in order to introduce inelastic scattering and dissipation within the bulk region (see separate sub-section below). Ando *et al* have been able to control the amount of inelastic scattering by controlling the coupling to these reservoirs while in our case we consider the full inelastic and incoherent case. But in contrast, we do not need to introduce artificial elements for introducing inelastic scattering, because this is already incorporated in the formal description of our nodes.

As will be also shown in this paper, the tunnelling process is well represented by the backscattering function $P(\Delta\nu)$ used in [85]. It can be calculated locally at the designated grid points from the magnetic field and the local carrier density. On this basis it is possible to model the shape of the sample by shaping the lateral carrier distribution. In this way it has been

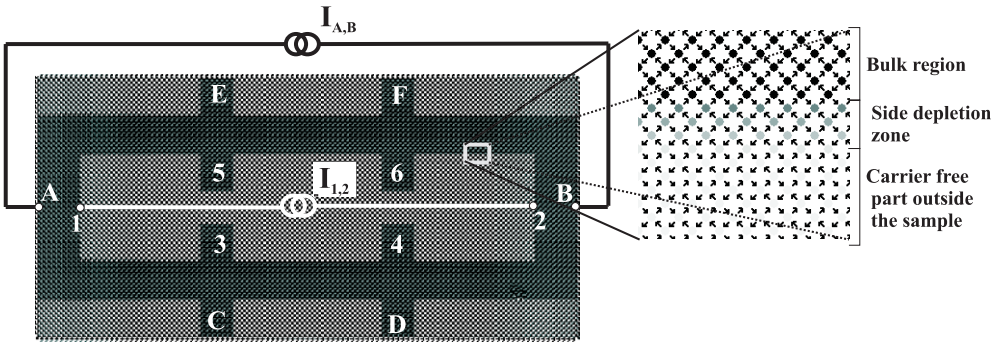

Figure 9. Sample layout for the network model of the 'anti-Hall bar within a Hall bar' geometry with two independent current sources, $I_{A,B}$ and $I_{1,2}$. The network consists of interconnected nodes with each of them representing a saddle point as shown in figure 7. These saddle points appear as shaded circles, with the grey scale applied towards indicating the local carrier density. The arrows, which are only visible in the expanded portion of the figure, represent the incoming and outgoing channels. The area with dark nodes indicates a constant carrier concentration of $n_0 = 4 \times 10^{11}$ cm^{-2}, which defines the bulk region of the sample. The gradual transition from dark grey to light grey represents the side depletion zone, from the bulk to zero carrier density at the sample boundaries (see the expanded portion of the figure). The current contacts are indicated by white dots at the inner and outer boundaries of the sample. The Hall voltages are measured between the voltage probes (3, 5) for the 'anti-Hall bar' and between (C, E) for the Hall bar. The corresponding longitudinal voltages are measured between the voltage probes (3, 4) for the 'anti-Hall bar' and (C, D) for the Hall bar.

shown for the first time that the influence of sample geometry (such as contact arms) and carrier density inhomogeneities (as introduced by gate electrodes) can be successfully addressed in full agreement with experimental results [85, 90, 113]. As an example of the high degree of complexity in the sample geometry which can be handled by our network model, figure 9 shows the network layout, which has been recently used for simulating magneto-transport in a 'anti-Hall bar within a Hall bar' geometry [113].

While the main task of [85] was to present the technical aspects and examples for applications of our network model, one major purpose of this paper is also to provide the theoretical and physical background as well as the relation to alternative approaches. Since the network model is based on the idea of tunnelling between magnetic bound states at saddles of the interior potential landscape, a systematic study of this tunnelling process will be presented in section 3. The interesting question of whether or not there is a correspondence between the EC picture and the bulk current picture in terms of mixed phases will also be addressed in section 5.

2.3. The lattice model

With the term 'lattice model' we refer to a method of discretization, which is not necessarily based on the idealization of a particular conduction mechanism of the real two-dimensional electron system (2DES), as this is the case for our proposed network model or for the CC model in the context of magnetic bound states. The basic concept of the so-called lattice model is that the space (2DES) is divided into discrete cells and the system is described by a nearest-neighbour tight-binding Hamiltonian H. The hopping parameter V and the site energies E are taken to be constant for ideal conductors, while a randomization of the site energies allows us to introduce disorder (Anderson disorder). Inelastic scattering and dissipation is introduced

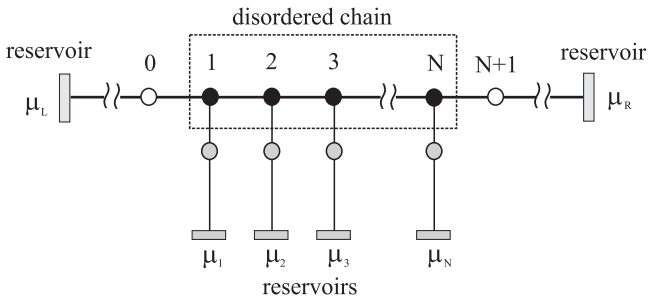

Figure 10. Schematic representation of a chain of disordered channels according to the model of D'Amato *et al* [128]. The chain extends from site 1 to site N (black circles) and is connected to the reservoirs μ_{L} and μ_{R} by perfect channels 0 and $N+1$ (white circles). Each site is connected to a reservoir (inelastic scatterer) by channels of controllable coupling (grey circles).

by coupling independent reservoirs to each lattice site via ideal conductors. The amount of inelastic scattering is controlled by the coupling of the lattice sites to the reservoirs. Hence, any mixture of coherent and incoherent transmission through the individual lattice sides is possible. The method of introducing inelastic scattering via coupled reservoirs was developed by Büttiker [126, 127] and has been applied to a conducting chain of disordered channels by D'Amato *et al* [128]. At this point only the basic ideas and their consequences for the introduced network models should be discussed. Therefore, for further details, refer to the cited literature.

As shown in figure 10, the conducting chain is connected to thermal reservoirs (μ_{L} and μ_{R}) by ideal leads and additionally the elements of the chain are coupled to individual thermal reservoirs, which can be understood as metallic voltage probes. This means that current conservation has to be assumed, which leads to the boundary condition of vanishing net current to and from the reservoirs $\mu_1 \cdots \mu_N$. The drawn connections between the scatterers in figure 10 represent just the coupling between the cells and must not be confused with the channels of a network model as in our case or the case of the CC model. Therefore, strictly speaking, the lattice model should not be attributed to the family of network models. However, the results of the lattice model are quite important for discussing the network models as well. The basis for the calculation is a nearest-neighbour tight-binding Hamiltonian and it delivers transmission coefficients, which are related to a conductance with the help of the Landauer formula. In this context transmission coefficients can be obtained for the whole system as well as for the single disordered channels, for which corresponding values of the two-terminal conductance can be given. However, it is important to keep in mind that the assignment of a two-terminal conductance to each lattice site does not automatically mean that the lattice can be turned into a resistor network. The inter-connections between the lattice sites must not be considered as current carrying channels, as one would expect from a circuit type network. In [128] it is shown that a single effective transmission coefficient T_{eff} can be obtained for the complete system, where incoherent as well as coherent transmission contributes. We interpret the existence of a single effective transmission coefficient T_{eff} as a very fundamental fact, because the two-terminal conductance of the system is calculated from T_{eff} without regarding to the individual contributions of coherent and incoherent transmission. If one asks e.g. for the total dissipation in the system, the conductance according to T_{eff} is used as usual, which means that for the totally dissipated energy the individual contributions of inelastic and elastic scattering seem not to be relevant. But this apparent inconsistency is easily resolved by the following argument: If we pass a constant current through the system (as usually done in experiments), we get dissipation

at the contacts and in the bulk of the conductor, which is heated by the inelastic scattering events. If we assume that just the elastic contribution to T_{eff} changes, the applied voltage to the current contacts has to adjust in order to keep the current constant. This means at the same time that the dissipated power at the contacts changes as well. In other words, the effect of elastic scattering in the conductor is incorporated in an additional power dissipation at the contacts, remote from the elastic scattering centres. For the total power dissipation of the system (without regard to the location of power dissipation) it is not relevant to which degree the contributions to T_{eff} are elastic or inelastic. However, it is important to realize that this argument only holds if the contacts are considered and treated as part of the system, which is the case in the lattice model as well as in our proposed network model, but this is not the case in the CC-model.

A two-dimensional version of the lattice model for the case of high magnetic fields has been applied by Ando *et al* [118]. Ando used this model for studying the voltage distribution in the bulk in the QH-regime [119]. Since the nearest neighbour sites communicate by coherent transmission via quantum states, these states acquire a phase change between the different sites due to the magnetic field (Peierls' phase factor for incorporating the effect of a magnetic field). In order to account for the LL broadening, Ando introduced additionally an appropriate fluctuation of the site energies. In this way Ando was able to study the QH regime in the vicinity of the plateau transitions as a function of the strength of inelastic scattering. We get an almost perfect agreement between the lateral voltage distribution obtained by Ando for the case of strong inelastic scattering and that obtained on the basis of our network model (see figures 22 and 23 in section 4). Against this background our network approach seems to serve as an alternative representation of Ando's lattice model for magneto-transport in the regime of strong inelastic scattering. However, it has to be left to the ongoing work to find also a theoretical link between the formal description of our network model and Ando's application of the lattice model. Once more it should be pointed out that in the discussed lattice model inelastic scattering has to be artificially introduced by individual reservoirs coupled to the lattice sites, while in our network model a possible dissipation due to inelastic scattering is already built in in the formal description of the nodes. However, our model at present considers incoherent transmission only, while the lattice model allows any mixture of coherent and incoherent transmission. In contrast, the CC model has no handle to account for dissipation at all.

2.4. The Chalker–Coddington network in the context of circuit type simulations

As already mentioned, the CC model was originally aimed at calculating the localization length of the electronic states in the QH regime, while our network model is directly aimed at modelling the distribution of experimentally excited currents and voltages. However, the CC model also attributes currents to the channels, which leads to the interesting question of whether therefore the CC model is also able to model such current and voltage distributions, as one would expect at first glance. To answer this question, we have first to consider one essential problem, which is not directly addressed by the transfer matrix of the CC network. On the one hand, the transfer matrix is formulated to relate amplitudes on the left to transmitted amplitudes on the right, which also should hold for the associated currents. On the other hand, in a situation without external current injection (equilibrium condition) the net current transfer across the node should be zero. This means that in equilibrium the transfer process from left to right must be compensated by a transfer process from right to left. This is schematically indicated in figure 11. We can expect that at least for vanishingly small deviations from equilibrium the transmission and reflection coefficients remain the same as for equilibrium (linear transport regime). Experimentally injected small currents can be considered as small deviations from

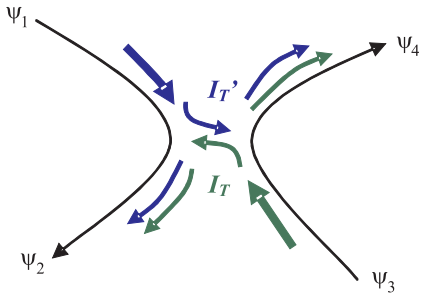

Figure 11. Schematic illustration that transfer from left to right should exist simultaneously with transfer from right to left, leading to a current balance at the saddle.

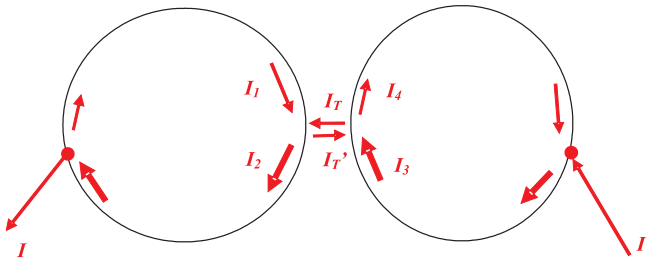

Figure 12. Schematic representation of two magnetic bound states which couple at a single saddle. The dots are the contacts for current injection and current extraction.

equilibrium and as such this should be incorporated by a balance of transmitted currents from left to right and from right to left. However, such a current balance is not directly incorporated by the transfer matrix itself. In order to produce a non-equilibrium case, one needs to inject a current by contacts, which is schematically shown by figure 12. We consider two magnetic bound states which get coupled across a single saddle. Without any further saddles the involved channels can only be a part of a closed loop as shown in the figure. The transfer matrix tells us the transmission at the saddle from left to right. The choice of this direction is arbitrary and consequently the transfer matrix also works in the reverse direction, which is achieved by the symmetry of this matrix. In order to look for experimentally observable effects we have now to excite a non-equilibrium current via the contacts. For a net current flow across the saddle we consider now the current balance between the transmitted currents I_{T} and I'_{T} from both sides of the saddle point. Based on figure 12 and using transmission and reflection coefficients for the currents ($T \propto t^2$ and $R \propto r^2$) we have to write the following:

$$I_{\mathrm{T}} = T I_3 \tag{14a}$$

$$I'_{\mathrm{T}} = T I_1. \tag{14b}$$

The net current I across the saddle, which has to be supplied experimentally, is the balance of the transmitted currents:

$$I = I_{\mathrm{T}} - I'_{\mathrm{T}} = T(I_3 - I_1). \tag{15}$$

This means for the current difference $I_3 - I_1 = I/T$. Already from this it becomes clear that the experimental current I cannot simply be injected exclusively into channel 3, because this would require that I_3 and I should be the same, in contradiction to the above equation. Furthermore, it also becomes clear that the currents, which are associated with the channels on the basis of the transfer matrix, must not be misinterpreted as experimentally injected currents.

However, it is anyway topologically impossible to attach a metallic contact to just a single channel like e.g. channel 3. Channel 3 is part of a magnetic bound state, which means that channels 1 and 2 of figure 4 are completed to a loop as well as channels 3 and 4 (see figure 12). Only on those loops can metallic contacts be attached (marked by the dots in figure 12). We inject a current I on the right side and extract it on the left side. Based on the CC model current I_3 gets split at the node into a transmitted component I_T and into a reflected component I_4. The same applies for the current I_1, which gets split at the node into a transmitted component I'_T and into a reflected component I_2. The net current flow is now the difference between the transmitted currents I_T and I'_T. With the help of figure 12 the current balance can be completed as follows:

$$I = I_3 - I_4 = I_2 - I_1 \tag{16}$$

which is equivalent to

$$I_1 + I_3 = I_2 + I_4. \tag{17}$$

At the first glance this looks like a proof of the CC model to hold also for the case of an injected non-equilibrium current. But this is not true because from equations (15) and (16) one can easily obtain the following inequality:

$$I_3 > \frac{I_3 - I_4}{T}. \tag{18}$$

This inequality holds in every case, because all currents are considered according to the direction of the channels and therefore only absolute values of the currents need to be considered and no change of sign can occur. The above inequality definitely tells us that the experimentally injected current I determines only the difference between I_3 and I_4 but not directly the absolute value of I_3, which may be considerably larger than the injected current I. On this basis the current I_3 can be only a mixture of the injected current I and a not necessarily known persistent current. This demonstrates quite clearly that the transfer matrix does not explicitly handle the distribution of experimentally injected (non-equilibrium) currents. Another most important aspect is the fact that besides the injected non-equilibrium current an excitation potential is required in order to inject this current. This excitation potential has to drop partly at the contacts, and as far as inelastic events are involved it also has to drop partly at the tunnelling junction at the saddle point. Since the CC model definitely assigns currents to the directed channels, there is no handle to address the transmitted potentials or a possible potential drop. Since the transfer matrix considers coherent transmission, the effect of dissipation due to inelastic scattering is not included in the formal description of the nodes in the CC model. As already mentioned above, a randomization of the phases of the wavefunction amplitudes which are transmitted between the nodes is introduced in the CC model, which, in our opinion, must not be misunderstood as an introduction of inelastic scattering. However, as long as equilibrium conditions are discussed, as in the original paper of Chalker and Coddington, this does not matter. At present we cannot see how experimental non-equilibrium situations could be addressed on the basis of the transfer matrix of the CC network even for vanishingly small injected currents.

2.5. Resistor network

Since our proposed network approach is also able to address the Ohmic regime of the plateau transitions, we compare our network with a resistor network and check for the possibility to represent our network in terms of a resistor network. As shown in figure 8, the minimum network consists of four nodes and resembles a single magnetic bound state. Considering two

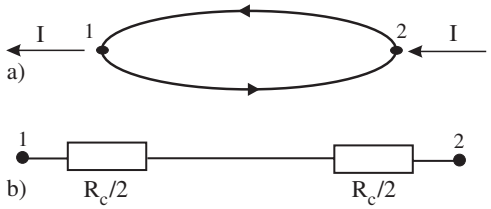

Figure 13. (a) Schematic representation of a magnetic bound state without any coupling to the environment and with two ideal contacts. The current is given by $I = (u_2 - u_1)e^2/h$ and u_2 is carried by the upper branch and u_1 is carried by the lower branch. (b) Equivalent circuit representation of the two-terminal resistance $R_{12} = h/e^2$, which must be associated with the presence of the contacts ($R_C = R_{12}$).

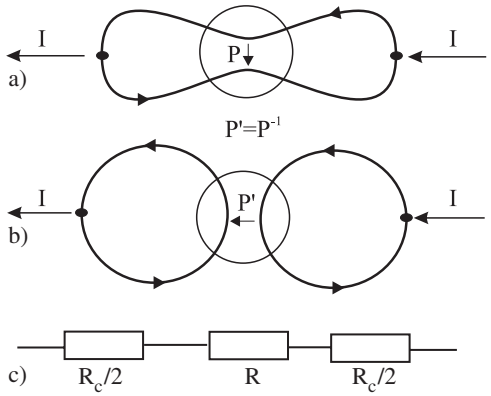

Figure 14. (a) Schematic representation of a magnetic bound state with the possibility of backscattering. The contribution of the backscattering to the longitudinal resistance R is given by $R = PR_{xy}$, which is for a single channel $R = R/Th/e^2$. (b) The same situation as in (a) can be represented by $P' = P^{-1}$ and turning the node by 90°. (c) Equivalent circuit representation of the two-terminal resistance R_{12}, which in this case must be composed by R_C and R.

contacts for current supply and assuming zero backscattering between the upper and lower branch of the loop, this element would represent a two-terminal resistance of h/e^2. Using an equivalent circuit, this resistance value has to be attributed exclusively to the presence of the metallic contacts. This is schematically shown in figure 13, where (a) shows a magnetic bound state with contacts and (b) shows the corresponding equivalent circuit in terms of Ohmic resistors. The next step of a generalization is considering a configuration in which the magnetic bound state experiences backscattering between the upper and lower branches of the loop (figure 14). The effect of backscattering is represented by an Ohmic part R in addition to the contact part R_C. The total two-terminal resistance between the current contacts is the sum of R_C and the Landauer type resistance R resulting from backscattering. This is easily checked by the following equations by calculating $R_{12} = R_C + R$:

$$R_{12} = \frac{h}{e^2} + \frac{R}{T}\frac{h}{e^2}. \tag{19}$$

This can easily be transformed into the two-terminal conductance:

$$G_{12} = T\frac{e^2}{h}. \tag{20}$$

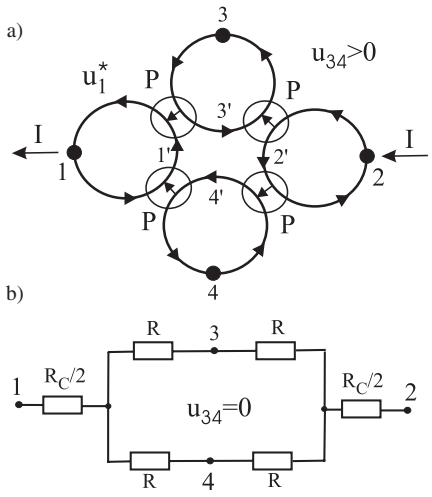

Figure 15. (a) Schematic representation of a network consisting of four coupled magnetic bound states. Additionally to the current contacts (1 and 2) also Hall voltage contacts (3 and 4) are attached. The opposite (inner) branches of the contacts are labelled according to $1'$, $2'$, $3'$ and $4'$. (b) Equivalent circuit representation of (a), where the coupling junctions between the loops are represented by two-terminal resistors ($R = (1/P)(h/e^2)$). While the two-terminal resistance R_{12} appears to be the same as for (a), the resistor network does not account for the Hall voltage between contacts 3 and 4, while our network does (see text).

Equation (20) is in full agreement with the Landauer conductance of a 1D channel containing a barrier of transmission coefficient T and with metallic contacts. From this point of view it seems possible to turn our network of coupled loops into a resistor network. However, as we will see, this does not work out for modelling magneto-transport. Let us assume a somewhat more complex network as shown in figure 15. It consists of four magnetic bound states coupled at four junctions in such a way that the total current gets distributed among more than just one channel pair. This model situation therefore can be considered as representative for the beginning of bulk current flow, where the current is distributed over a certain area instead of having a well defined channel pair taking all the current. The equivalent circuit is shown in figure 15(b) and it clearly indicates two alternative possibilities for current flow between the current contacts. Since in figure 15(a) the current flow is associated with a current across the junctions, this corresponds to a node description according to figure 14(b) and therefore the reciprocal value of P has to be used for calculating the associated resistance R of the junction, as explained in the caption of figure 15. Let us now analyse the situation on the basis of figure 15(a). As a first task we calculate the two-terminal voltage between the current contacts 1 and 2. The potential of contact 2 (u_2) is transmitted to the upper right node. For symmetry reasons the current across this node must be $I/2$ because half of I is transmitted across the lower right node. According to the EC picture the channel $2 \rightarrow 2'$ experiences a potential drop ($\Delta u = u_2 - u_2'$) while passing the node. This is given by

$$\Delta u = \frac{h}{e^2}\frac{I}{2}. \tag{21}$$

This allows us to calculate u_2':

$$u_2' = u_2 - \frac{h}{e^2}\frac{I}{2}. \tag{22}$$

According to the EC picture we also have $U_{xx} = PU_{xy}$ (see e.g. equation (11)), which means $(u_2 - u_2') = P(u_2 - u_3)$, and it allows us to calculate the potential drop across the upper right node of figure 15(b):

$$u_2 - u_3 = \Delta u / P. \tag{23}$$

Therefore, we finally get

$$u_3 = u_2 - \frac{h}{e^2}\frac{I}{2}\frac{1}{P}. \tag{24}$$

Now we can go on and ask for the potential u_1^* (not identical to u_1!). For this the same arguments as for obtaining u_3 from u_2 have to be repeated once more. This means that another potential drop of the same amount as from contact 2 to contact 3 appears. Therefore the total potential difference $u_2 - u_1^*$ is twice the amount appearing in equation (24):

$$u_2 - u_1^* = \frac{h}{e^2}\frac{I}{P}. \tag{25}$$

The total current, which is supplied by the contacts, has to be represented by the EC picture as well and therefore the following equation also holds:

$$I = (u_1^* - u_1)\frac{e^2}{h}. \tag{26}$$

We now use equation (25) for substituting u_1^*:

$$I = \left(u_2 - \frac{h}{e^2}\frac{I}{P} - u_1\right)\frac{e^2}{h}. \tag{27}$$

This allows us to calculate the two-terminal voltage between the current contacts:

$$u_2 - u_1 = \left(\frac{h}{e^2} + \frac{1}{P}\frac{h}{e^2}\right)I. \tag{28}$$

This means that the total two-terminal resistance consists of the contact resistance $R_C = h/e^2$ and a resistance R_N which can be associated with a representative resistance of the network without contacts ($R_N = P^{-1}h/e^2$). This result can be obtained on the basis of the equivalent circuit in figure 15(b) as well, because $R = P^{-1}h/e^2$ and the total resistance R_N of the four resistors of the network is again R. However, if we look for the Hall voltage u_{34}, the resistor network obviously gives a zero value. In contrast, the channel network of figure 15 gives a non-zero value, which we will calculate as follows. For symmetry reasons, the potential difference between contacts 1 and 4 is the same as the already calculated potential difference between contacts 2 and 3. This means that we have $u_4 - u_1 = u_2 - u_3$ and therefore we also have $u_4 = u_1 + \Delta u/P$. Together with equations (21)–(24) we can write

$$u_3 - u_4 = u_2 - \frac{1}{P}\frac{h}{e^2}\frac{I}{2} - u_1 - \frac{1}{P}\frac{h}{e^2}\frac{I}{2}. \tag{29}$$

Using further equation (28), we finally get

$$u_3 - u_4 = \frac{h}{e^2}I. \tag{30}$$

This is exactly the Hall voltage of a single LL. In contrast, it is quite clear that the associated resistor network is not able to account for this Hall voltage. This finally brings us to the conclusion that our network approach cannot be substituted by an Ohmic resistor network, even though we consider fully incoherent coupling at the nodes of our network.

3. The saddle-point problem

In the previous section we demonstrated that on the one hand our network approach is essentially different from the CC network because it does not take into account coherent transmission across the nodes of the network. On the other hand it also cannot be reduced to a simple resistor network. Another alternative approach is the lattice model as discussed above. However, the lattice model is more likely an abstract method of discretization of a 2DES without referring to a particular conduction mechanism of the real system, which would be needed as the basis for building up a circuit-like network. Our approach is based on the idea of transmission across magnetic bound states and therefore it is necessary to have a closer look at the physical background of our network model. This is done by reconsidering the problem of quantized transmission across saddle-point constrictions.

The problem of quantized transmission across a saddle-point constriction with magnetic field has been addressed in the past by Büttiker [129]. Büttiker's paper was motivated by the theoretical discussion of quantized conduction steps discovered by van Wees *et al* [20] and Wharam *et al* [21] in split gate constrictions of a two-dimensional electron gas. Since constrictions in these experiments are electrostatically induced with a pair of split gates, the potential is a smooth function (without hard walls) and the bottleneck of the constriction therefore forms a saddle. At this point our view of the role of potential fluctuations meets the split gate situation referenced above. In this context we look for a link between the results of Büttiker for the bottleneck situation at high magnetic fields and our semi-empirical backscattering function $P(\Delta\nu)$. Following the paper of Büttiker for the high magnetic field limit, the trajectories of the states are given by equipotential lines defined by $\varepsilon = eV(x, y)$, where ε denotes the energy of the guiding centre of the classical cyclotron orbit, V the potential and e the electron charge. If V_0 denotes the potential of the saddle, the case $\varepsilon < eV_0$ describes a trajectory which is repelled by the saddle, where the energy ε is finally represented by the Fermi level. Using the considered saddle point as the centre of our coordinate system, the minimum distance y_n between trajectories of the same energy, which are classically repelled on opposite sides to the saddle point, is determined by $\varepsilon = eV(0, y_n)$ for $\varepsilon < eV_0$ (see figure 16). A similar situation appears for $\varepsilon > eV_0$, but turned around by 90°, and the minimum distance x_n is determined by $\varepsilon = eV(x_n, 0)$. According to Büttiker, the transmission probabilities in terms of x_n and y_n in the high magnetic field limit for the case of $\varepsilon_n > 0$ are

$$T_{mn} = \delta_{mn}\left\{1 + \exp\left[\pi\frac{\omega_x}{\omega_y}\left(\frac{x_n}{l_B}\right)^2\right]\right\}^{-1} \tag{31}$$

and for the case $\varepsilon_n < 0$

$$T_{mn} = \delta_{mn}\left\{1 + \exp\left[\pi\frac{\omega_y}{\omega_x}\left(\frac{y_n}{l_B}\right)^2\right]\right\}^{-1}. \tag{32}$$

The underlying problem is basically a tunnelling problem and δ_{nm} tells us that this tunnelling process with the tunnelling rate T_{mn} happens mainly between the same states (states of same LL) on opposite sides of the saddle. The parameters ω_y and ω_x result from expanding the potential near the saddle point by

$$V(x, y) \approx V_0 + 0.5m\omega_x^2x^2 - 0.5m\omega_y^2y^2. \tag{33}$$

Now we look for a relation between the transmission rates given above and the function $P(\Delta\nu)$, which represents the ratio between transmission and reflection R/T of edge states as used in the network model. If we look for x_n while $y_n = 0$ ($\varepsilon_n = e(V - V_0) > 0$), we can easily calculate x_n from equation (33):

$$x_n^2 = \frac{2\varepsilon_n}{m\omega_x^2}. \tag{34}$$

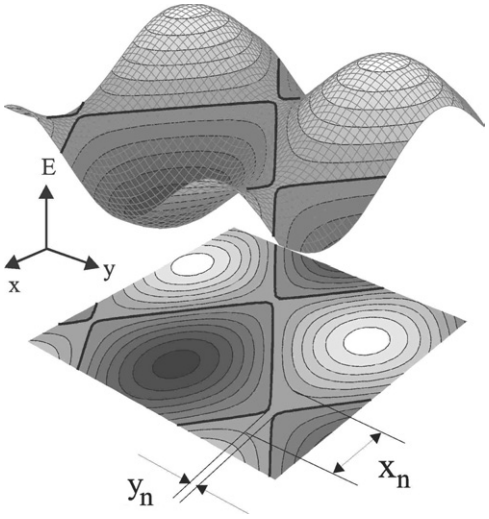

Figure 16. Example for a two-dimensional potential modulation which forms saddle points. The minimum distances of the closed loops (magnetic bound states) are shown for two different cases: y_n is achieved if ε is below the saddle energy eV_0 (bold line) and x_n is achieved if ε is above the saddle energy. All possible loops represent equipotential lines and the selection of the active loops is made by the position of the Fermi level ($\varepsilon = E_F$).

In the case $\varepsilon_n < 0$ we get something analogous for y_n^2:

$$y_n^2 = \frac{2\varepsilon_n}{m\omega_y^2}. \tag{35}$$

We introduce an artificial periodic potential modulation, which is a two-dimensional cosine function and which has the same Taylor expansion as equation (33):

$$V(x, y) = \tilde{V}[\cos(\omega_y y) - \cos(\omega_x x)] \tag{36}$$

with $\tilde{V}$ being the potential modulation. The saddle energy of this potential is zero ($V_0 = 0$). Figure 17 shows a contour plot of the two-dimensional cosine potential modulation and we get a saddle point whenever the maximum of the cosine in one direction meets a minimum of the cosine in the other direction. In this way we get a periodic array of saddle points. We consider one saddle to be located exactly at the origin of our coordinate system. If we think about a smoothly varying random fluctuation potential, the average curvature in both directions will be the same. In our representative potential in equation (36) we therefore simplify by setting $\omega_x = \omega_y = \omega$, which leads to $\omega_x/\omega_y = 1$. In order to re-write equations (31) and (32) we make some further substitutions. For the magnetic length l_B we use

$$l_B^2 = \frac{h}{2\pi eB} \tag{37}$$

with h the Planck constant, e the electron charge and B the magnetic field. Using further the period length L of the periodic arrangement of saddle points

$$L = 2\pi/\omega \tag{38}$$

we can rewrite equations (34) and (35):

$$x_n^2 = \frac{L^2\varepsilon_n}{2\pi^2 e\tilde{V}} \tag{39}$$

$$y_n^2 = \frac{L^2\varepsilon_n}{2\pi^2 e\tilde{V}}. \tag{40}$$

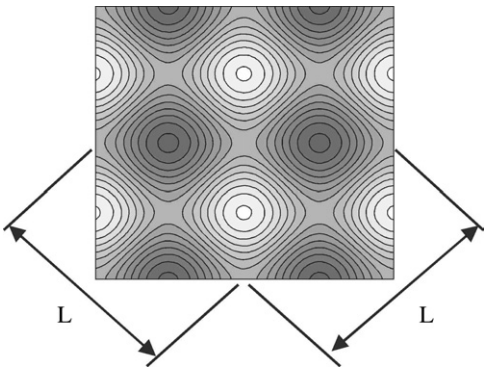

Figure 17. Contour plot of the artificial 2D cosine potential. Dark indicates potential minima and the light coloured areas indicates the potential maxima. L is the period of the potential modulation and at the same time it is the grid period of the network.

Equations (37)–(40) now allow us to re-write equations (31) and (32). Since x_n and y_n are described by exactly the same function, but distinguished only by the case ε_n either above or below the saddle energy, we can rewrite equations (31) and (32) into a single equation as follows:

$$T_{mn} = \delta_{mn}\left\{1 + \exp\left[\pm\frac{L^2\varepsilon_n}{e\tilde{V}}\frac{eB}{h}\right]\right\}^{-1}. \tag{41}$$

The signs $\pm$ indicate the cases ε_n above and below the saddle energy, while ε_n in this formula means the absolute value. At this point it should be mentioned that Haug *et al* [25] have already used a similar equation for addressing the problem of transport across magnetic bound states. They investigated experimentally the effect of a gate electrode across the current path of a QHE sample at constant magnetic field. The major point of that experiment was to study the special situation of having integer filling outside the gate (pure EC transport) and sweeping the gate voltage through non-integer filling below the gate. The authors describe the scattering across the bulk due to the presence of the gate by partly EC backscattering at the gate and partly backscattering via tunnelling across magnetic bound states in the gate region. They achieved good agreement with the experiments already by a simplified network consisting of just two or three magnetic bound states. In order to be able to compare with the formulation of EC backscattering in terms of $P(\Delta\nu)$, we have to realize that the transmission process across the saddle T_{mn} is formally a backscattering process in the EC picture. Therefore the transmission factor T_{mn} in equation (41) corresponds to a reflection R in the EC picture. We transform equation (41) into $P = R/T$ by using T_{mn} as R and consequently using $(1 - T_{mn})$ as T:

$$P = \frac{R}{T} = \frac{T_{mn}}{1 - T_{mn}}. \tag{42}$$

Since the above tunnelling process happens between edge states on opposite sides of the saddle but the same Landau level (LL), δ_{mn} can be omitted for the further treatment. Furthermore, we have to consider that the energy ε_n is determined by the Fermi level E_F. In this way we end up with P as an exponential function of the Fermi level E_F:

$$P = \exp\left[\mp\frac{L^2E_F}{e\tilde{V}}\frac{eB}{h}\right]. \tag{43}$$

In this equation E_F is the absolute value of the Fermi energy relative to the saddle energy and the signs $\pm$ indicate the cases E_F above and below the saddle energy. The ratio $L^2/\tilde{V}$ can

be understood as a measure of the 'smoothness' of the potential modulation and eB/h is the well known number of states in a single LL per unit area. Since L is the distance between equivalent saddle points, L^2 is the area of the two-dimensional basis cell of the network grid. It is interesting to note that the pre-factor of E_F, which is $(L^2/e\tilde{V})(eB/h)$, has the meaning of an average density of states (DOS) in the basis cell of the network, provided that we associate the LL broadening with $e\tilde{V}$. In order to consider this aspect in a little more detail, we assume a Gaussian shaped density of states for a single LL [109] and calculate the DOS in the centre of the LL as follows:

$$\mathrm{DOS}(\varepsilon_n = 0) = \frac{eB}{h}\frac{1}{b\sqrt{\pi}} \tag{44}$$

where b is the energy broadening of the Gaussian peak. Against this background we can calculate the change of the carrier density Δn in a single LL due to the change of E_F by ΔE_F as follows:

$$\Delta n = \frac{eB}{h}\frac{1}{b\sqrt{\pi}}\Delta E_F. \tag{45}$$

This is valid for a Fermi level close to the centre of the LL, where the DOS is approximately constant. However, we can also represent Δn in terms of the filling factor by $\Delta\nu = \Delta n/n_{LL}$, where $n_{LL} = eB/h$. This results in

$$\Delta\nu = \frac{\Delta E_F}{b\sqrt{\pi}}. \tag{46}$$

Using again the saddle energy as the zero reference, ΔE_F becomes E_F and $\Delta\nu$ becomes the difference of the filling factor relative to half filling. Now we can substitute E_F by $\Delta\nu$ and rewrite equation (43):

$$P = \exp\left[-\Delta\nu\frac{b\sqrt{\pi}}{e\tilde{V}}L^2\frac{eB}{h}\right]. \tag{47}$$

Since $\tilde{V}$ is the amplitude of our artificial potential modulation and b is the width of the associated DOS peak, these two parameters correspond to each other. Therefore we can assume that the pre-factors in the exponent will be a factor of the order of unity, just depending on details of the real potential fluctuations. On this basis we simplify

$$\frac{b\sqrt{\pi}}{e\tilde{V}} \approx 1 \tag{48}$$

and get the following exponential function:

$$P = \exp\left[-\Delta\nu L^2\frac{eB}{h}\right]. \tag{49}$$

It is easily seen that the semi-empirical exponential function of [71] is completely recovered, except the fact that we get a more complex pre-factor for the filling factor $\Delta\nu$. The explicit magnetic field dependence of the pre-factor is a new feature as compared to the earlier version of this function. However, this has no impact on the major features of the function $P(\Delta\nu)$, just causing a magnetic field dependence of the width of the plateau transition regimes. If we take a closer look at the exponent, we find eB/h, which is the number of states per unit area in an LL, and L^2, which is the area of a grid period of the network. As a consequence we get a surprisingly universal result. The exponent of the function $P(\Delta\nu)$ represents the number of carriers being added ($\Delta N > 0$) or removed ($\Delta N < 0$) from the half filled basis cell of the network grid. This happens if the Fermi level moves away from the centre position of the LL.

$$P = \exp\left[-\Delta N\right] \tag{50a}$$

$$\Delta N = \Delta\nu L^2\frac{eB}{h}. \tag{50b}$$

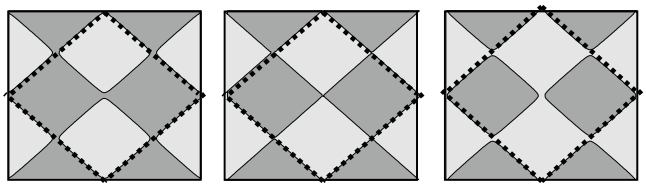

Figure 18. Spatial distribution of filled (dark coloured) and empty (light coloured) states for left, $E_F > E_{LL}$; middle, $E_F = E_{LL}$, and right, $E_F < E_{LL}$. The dotted line indicates the basis cell of the network.

This is usually achieved by changing the magnetic field at constant carrier density. However, this change normally happens continuously, meaning that the number of electrons in a single LL in one grid period is changed just in fractions of unity. This is possible because in the regime close to a half filled LL there is a strong coupling between the individual grid periods so that the (single) electrons are well de-localized and can be smeared over several grid periods. A change of the number of electrons by $\Delta N = \pm 1$ corresponds to an almost complete plateau-to-plateau transition. By considering the grid period length L as a measure of the smoothness of the potential fluctuations, we get a nice possibility for an interpretation of our result: a large L corresponds to a rather clean sample (high mobility) with very smooth potential fluctuations and a short L corresponds to a sample with strong potential fluctuations and hence strong disorder (low mobility). As a consequence, a large L indicates a large area of the basis cell of the network and therefore only a small change of the filling factor $\Delta\nu$, and thus only a small change of the magnetic field is needed in order to change the number of electrons in the basis cell by one. This means that we get sharp plateau-to-plateau transitions on the magnetic field axis. In contrast, a small L, as expected from samples with strong disorder, leads to a small area of the basis cell, which then requires a large change of the filling factor $\Delta\nu$ for changing the number of states by the order of one. Therefore we get broad plateau-to-plateau transitions in this case, exactly what we expect for samples with strong disorder. On the basis of geometric arguments and using a chequerboard as representative for the network (figure 18), equation (50) also allows another interesting interpretation: using directly the trajectories of the channels at different Fermi levels we get three cases as shown in figure 18: (i) if the Fermi level is above the saddle energy (centre of LL), the filled states dominate the transport properties, because they build an interconnected network; (ii) if the Fermi level coincides with the saddle energy, filled and empty states take up exactly half of the space, which also means an exactly half filled LL; (iii) if E_F is below the saddle energy, the empty states (insulating phase) build an interconnected network, leaving isolated droplets of filled states and leading to a high resistivity regime. It should be mentioned that Mashida *et al* have already used such a picture for the interpretation of their experimental results [51, 95].

4. Some simulation results

In this section we present some representative simulation data in order to demonstrate the potential of our model. An additional example can be found in [113], for which the network layout has been already used as an example in figure 9. In contrast to previous simulations, we use equation (49) as a replacement of the original function of [85] and we get results for the magneto-transport simulation as shown in figures 20 and 21. The layout of the sample is shown in figure 19. The network has a grid size of 139×53 and the bulk carrier density is 4×10^{11} cm^{-2}. Considering the individual plateau transitions at high magnetic fields, there

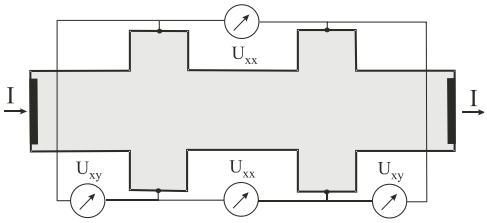

Figure 19. Sample layout as used for the numerical simulations.

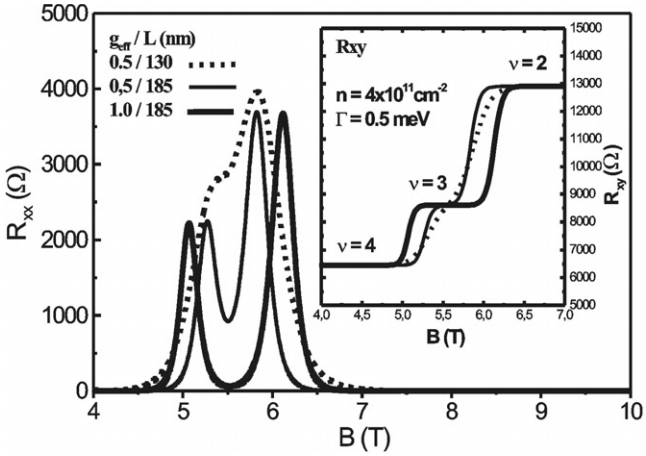

Figure 20. Results for magneto-transport data in the high field regime calculated with equation (49) as the function for P in the coupling function for the nodes of the network. The calculation is done for two different effective g-factors ($g_{\rm eff} = 0.5$ and $g_{\rm eff} = 1.0$) and two different values for $L = 130$ and 185 nm, which serve as the typical lateral extension of the long range potential fluctuations.

is no qualitative difference from the results of the previous version. The major difference and improvement concerns the low magnetic field range. At very low magnetic fields the zeros in R_{xx} disappear and the Hall effect starts as a straight line, and turns gradually over to a plateau behaviour at higher fields. The reason for this is the explicit magnetic field dependence of the exponent in equation (49), which results in an overlap of the Ohmic (dissipative) regimes of several LLs at low fields. In order to get the individual filling factors in the case of LL overlap, the individual spin-split LLs have been calculated using the standard parameters for GaAs and an LL broadening according to $\Gamma = \Gamma_0\sqrt{B}$ [109] has been used by setting $\Gamma_0 = 0.5$ meVT$^{0.5}$. The actual calculation consists of two main parts. (I) For calculating the occupation numbers standard procedures are used and the Fermi level in the bulk region is calculated by filling up the density of states (DOS) with the constant bulk carrier density. The DOS is composed by the superposition of the magnetic-field-dependent Gaussian shaped DOS of spin-split LLs. The Fermi level for regions of non-zero electrostatic bare potential (edges and gate regions) is forced to match the obtained magnetic-field-dependent pinned Fermi level in the bulk. This allows us to get a self-consistent electrostatic potential and a rearrangement of the carrier density at the edges, which results in an electrostatic edge potential according to Chlovskii *et al* [2]. (II) The thus obtained lateral carrier density profile is transferred to the nodes of the network and in another self-consistent iteration procedure the lateral distribution of the bias voltage, which is

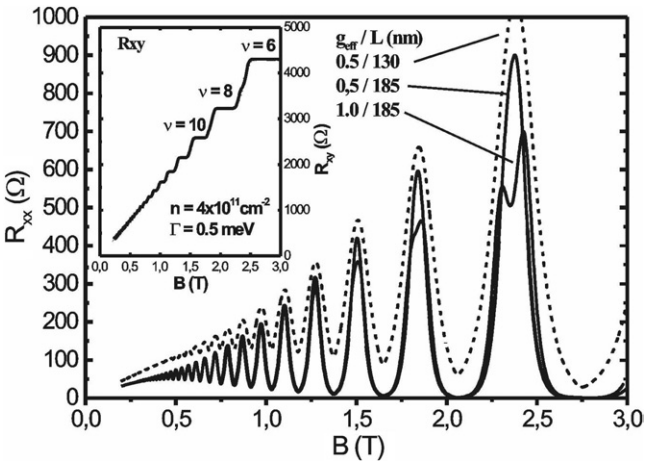

Figure 21. Results for magneto-transport data in the low field regime calculated with equation (49) as the function for P in the coupling function for the nodes of the network. The calculation is done for two different effective g-factors ($g_{\mathrm{eff}} = 0.5$ and $g_{\mathrm{eff}} = 1.0$) and two different values for $L = 130$ and 185 nm, which serve as the typical lateral extension of the long range potential fluctuations.

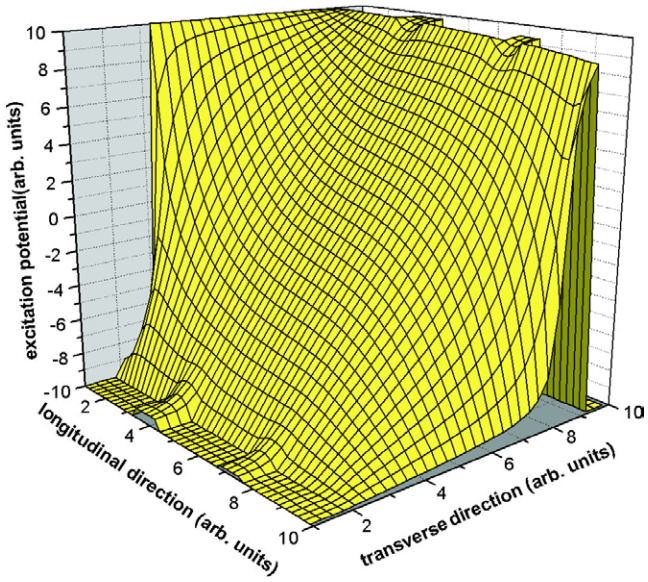

Figure 22. Simulation results showing the lateral distribution of the excitation potential for a single nearly filled LL. The layout is qualitatively the same as shown in figure 19.

introduced via the current contacts, is calculated. From this the potential difference for any designated pair of voltage probes is obtained as a function of the magnetic field. A metallic contact is realized by interconnecting all channels of all involved LLs at the position of the designated contact point [85]. Extended metallic contacts are realized by creating arrays of such contact points. The current at the current contacts is calculated only after arriving at the self-consistent solution in the network, which allows us finally to calculate the various resistances. This means that in principle a constant supply voltage is used in the network model instead of

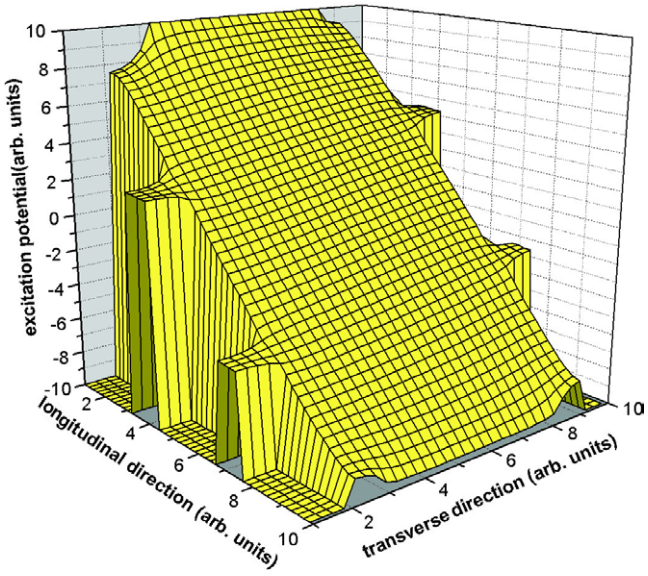

Figure 23. Simulation results showing the lateral distribution of the excitation potential for a single nearly empty LL.

a constant supply current as in most experiments. However, for calculating the resistances for a standard QHE set-up with a single current source this makes no difference. For achieving a constant current mode, the potentials at the current contacts are additionally varied in a proper way during the iteration procedure in order to get the required preset current. In this way a one-to-one simulation of experiments using constant supply currents and measuring voltages at several potential probes is possible.

Just for demonstration, the influence of spin splitting by using different effective g-factors such as $g^* = 0.5$ and $g^* = 1.0$ and different values for L, such as $L = 135$ and 185 nm, is simulated. These values for L are chosen in agreement with the extension of the lateral potential fluctuations which one can expect in real 2D systems. These therefore would also become the typical droplet size of the breaking-up electron sea, if the Fermi level enters the tails of the LL, in agreement with the model developed in section 3. According to this transport model, the associated potential fluctuations are also responsible for the set-in field of the SdH oscillations at about 0.3 T, which are smeared out completely below that field. This effect, in our model, is driven by an overlap of the de-localized states of several overlapping LLs at low fields due to the built-in inhomogeneities. In real systems, such an effect could in principle cover any scattering limited mechanisms for the set-in field of the SdH oscillations. The results are shown in figure 20 for the high magnetic field range and in figure 21 for low magnetic fields. For $L = 135$ nm and $g^* = 0.5$ spin splitting is hard to observe even at high fields around 5 T, while for the case $L = 185$ nm a well resolved spin splitting can be observed even for $g^* = 0.5$. At magnetic fields around 2.5 T spin splitting is only weakly pronounced even for $g^* = 1$ and $L = 185$ nm. In summary, one can say that this overall behaviour looks quite realistic and a more systematic study on the possibility of a more accurate determination of an enhanced effective g-factor from transport data is planned separately.

As already mentioned in the context of the lattice model in section 2, we see our network model as more closely related to the lattice model for the case of strong inelastic scattering than related to the CC model. In order to demonstrate this aspect, in figures 22 and 23 we

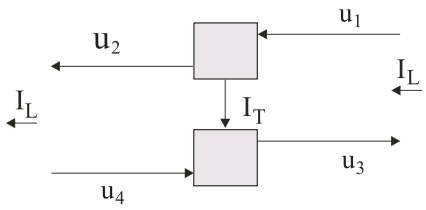

Figure 24. Schematic representation of the effect of backscattering in the EC picture.

present simulation results for the lateral distribution of the excitation voltage for a single LL for the case of a nearly filled LL and a nearly empty LL. The results agree perfectly with the results of Ando *et al* for the case of strong inelastic scattering [119]. The major difference from Ando's simulations is the presence of extended current injecting contacts in our case. This prevents the full development of the Hall voltage near the current contacts in figure 22, as also known from real experiments. However, the region between the voltage probes shows a nearly perfect Hall potential. At the same time this demonstrates that our model is able to account for the boundary conditions like the presence of contacts. The weak longitudinal potential drop in figure 22 results from the fact that the LL is not completely filled in this simulation. For the case of a nearly empty LL (figure 23) the presence of the extended current contacts does not harm the longitudinal potential drop, which agrees perfectly with Ando's calculation results. Since the current contacts are not extended over the full width of the sample, minor departures from the ideal voltage distribution occur at the corners near the current contacts. In both figures 22 and 23 the current contacts at the front side have been cut away in the potential plot. The sample layout is qualitatively the same as shown in figure 19, but in order to get a better resolution of the lateral potential distribution the number of grid periods for the bulk region is increased to 179×129 as compared for the calculation in figures 20 and 21. For this simulation smaller contact leads for the voltage probes have also been used. One can clearly see that for the high resistive case of a nearly empty LL these voltage probes act as classically expected, which means that they are current-less at constant potential. For the case of mixed EC and bulk transport, this may not be always the case, like demonstrated in [90].

5. Discussion

By using a representative two-dimensional cosine potential modulation, a result by Büttiker [129] for the saddle point problem at high magnetic fields was transformed into the back-scattering function $P(\Delta\nu)$, which is used for the nodes of our network according to [85]. One main extension as compared to [129] is the treatment of the tunnelling current within the framework of the Landauer–Büttiker formalism. This means that a transverse current between a channel pair (tunnelling current serves as a backscattering current between channels) leads to a longitudinal potential drop in each of the channels. This can be considered as the essence of the EC picture within the LB formulation and there is no classical way to account for this behaviour. In order to point out this fact somewhat more clearly, the situation is sketched in figure 24. If there is a longitudinal current I_L, it is carried dissipation-less by a channel pair and is represented on the right side by $I_L = (u_1 - u_3)e^2/h$ and on the left side by $I_L = (u_2 - u_4)e^2/h$, while $(u_1 - u_3) = (u_2 - u_4)$ for current conservation reasons. A transverse current I_T, which may be enabled by some conduction or tunnelling between opposite channels, causes a longitudinal voltage drop $(u_1 - u_2)$ and $(u_3 - u_4)$. This is because I_T also has to be represented within the LB formalism according to $I_T = (u_1 - u_2)e^2/h$ at the upper edge and

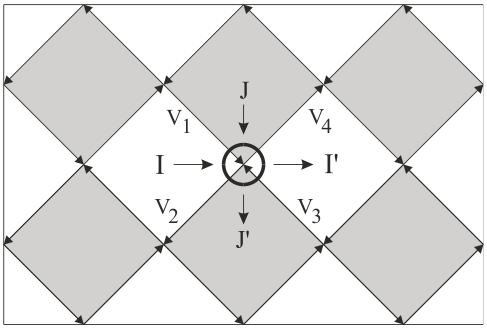

Figure 25. Checkerboard model for bulk current transport in the QHE regime after Ruzin *et al* [12]. The dark and light areas represent different quantum Hall liquids with different Hall conductances. Currents I and J are assumed to flow exclusively in the corresponding phase and the total behaviour of the conductor is determined by the mixture of both phases.

$I_T = (u_3 - u_4)e^2/h$ at the lower edge, while $(u_1 - u_2) = (u_3 - u_4) = \Delta u_L$, again because of current conservation reasons. It is important to note that any current (I_L or I_T) within the EC picture is only defined by a pair of directed channels, which must not be confused with a difference of opposite directed classical currents. As a consequence, it is not possible to assign a current to any single directed channel, and the occurrence of a transverse current I_T does not change the longitudinal current I_L. This is a fact which must not be misinterpreted as a violation of Kirchhoff's law of current conservation. Using finally the ratio I_T/I_L as an equivalent for R/T of the LB formalism, it is easily shown that the longitudinal voltage drop Δu_L is coupled to the Hall voltage as $\Delta u_L = (u_1 - u_2) = (u_1 - u_3)R/T$, with R/T identified as P, the function derived in this paper and used for the nodes in our network model.

The above summarized view of the EC picture has already been used in [60] in order to explain an anomalous behaviour of the magneto-transport of high mobility quasi-three-dimensional PbTe wide quantum wells. Also in [71] this interpretation of the EC picture has been successfully used, which finally led to the application within the discussed network model. From this point of view the network model can be considered to be based on the EC picture and the LB formalism. It is therefore quite surprising that the Ohmic regime is also quite well represented. However, this puzzle can be resolved by reconsidering figure 18, which appears like a chequerboard representation of the network. From this point of view it meets the approach of Ruzin *et al* [12]. Ruzin *et al* used such a chequerboard model for bulk transport in the QHE regime in order to obtain a universal relation between longitudinal and transverse conductance in the QHE and figure 25 summarizes their concept. Ruzin *et al* considered two competing quantum Hall liquids in the presence of a long-range random potential, with the magnetic field determining the area fractions close to 1/2. Figure 25 represents this situation for an artificial periodic long-range potential. The 'white' regions represent the phase with quantized Hall conductance σ_1, and the 'dark' regions those of Hall conductance σ_2. If the situation is such that the 'white' phase percolates freely throughout the sample, the system will be on the plateau with $\sigma_{xy} = \sigma_1$. Similarly, if the 'dark' regions percolate freely, the system will be on the plateau with $\sigma_{xy} = \sigma_2$. Near the percolation threshold transport is controlled by quantum tunnelling between clusters of the same phase at the saddle points. Ruzin *et al* related the net currents in the four quadrants to the four electric potentials at the edges V_1 through V_4 as given by

$$I = \sigma_1(V_2 - V_1) \tag{51a}$$

$$J = \sigma_2(V_3 - V_2) \tag{51b}$$

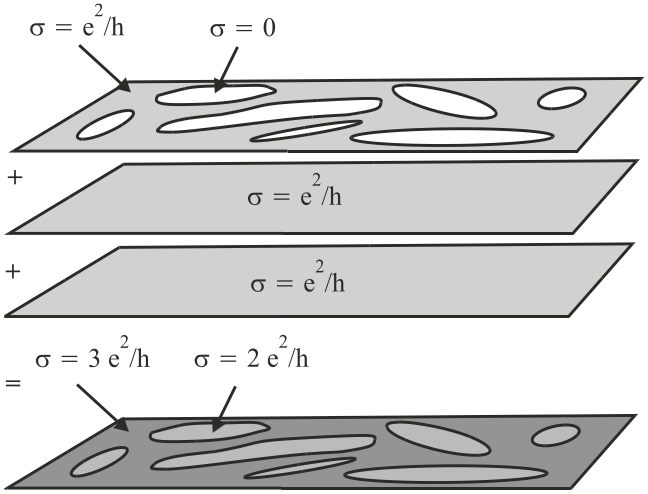

Figure 26. Scheme for combining individual LLs, where each of them may have a mixture of quantum Hall liquid and insulating phase. In this case it is assumed that just the top LL is partly occupied and all lower ones are completely filled. The result is a combined system of mixed phases of different quantum Hall liquids of different Hall conductivities.

$$I' = \sigma_1(V_3 - V_4) \tag{51c}$$

$$J' = \sigma_2(V_4 - V_1). \tag{51d}$$

Postulating current conservation within the individual phases ($I = I'$ and $J = J'$), Ruzin *et al* get automatically $(V_2 - V_1) = (V_3 - V_4)$, which is identical to the results of our treatment as illustrated in figure 24. Further on, Ruzin *et al* obtained a universal semi-circle-relation between longitudinal and transverse conductance. At this point it should be mentioned that such a semicircle relation has also been obtained within our preceding work [68, 71], which once more demonstrates the agreement of our results with the results of Ruzin *et al*. However, our model achieves additional results, such as the filling factor dependence and transport parameters in terms of R_{xx} and R_{xy} as well as the distribution of the applied voltage across the sample area. There is also a qualitative difference between Ruzin's and our picture: in our picture the space is divided between occupied and non-occupied states, while Ruzin *et al* are talking about two competing quantum Hall liquids (QHLs) of different Hall conductivities. We can overcome this disagreement by recognizing that in our model each involved LL is represented by a separate network with its individual mixture of empty and filled states, which we associate with the insulator phase and the quantum Hall liquid (QHL) phase respectively. In the case of the IQHE there is always just one partly filled (top) LL and all lower ones are completely filled. For each LL the QHL phase exhibits a quantized Hall conductance of $\sigma = e^2/h$, while the Hall conductance for the insulator phase $\sigma = 0$. For the complete system in the bulk current representation we have to sum up all contributions of all LLs locally, which leads to a situation as sketched schematically in figure 26. Putting forward a bulk current representation, one has to sum up the Hall conductivity of all involved LLs locally and the resulting picture becomes again similar to that of Ruzin *et al*. At this point we want to make clear that at this stage our network model does not include non-linear effects, which means that it considers the electron system to be sufficiently close to thermal equilibrium. However, for thermal equilibrium some similarity between the bulk and edge current picture might not be that surprising. A recent theoretical treatment of non-linear transport through mesoscopic systems by Sanchez *et al* [104] shows

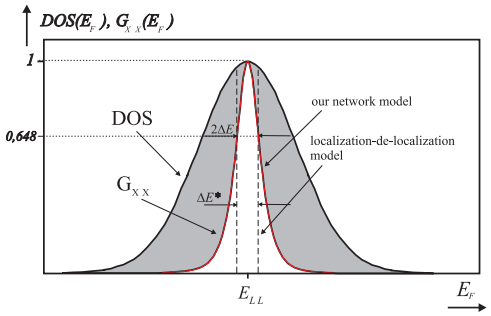

Figure 27. Function plot for the DOS and G_{xx} versus Fermi energy relative to the LL centre. Both plots are normalized to each other. This plot exhibits striking similarities with the localization–de-localization model of the quantum Hall plateau transitions, where the DOS is divided into localized and de-localized states by an energy interval as indicated by the two vertical dashed lines. In this context our model suggests a smooth transition between localized and de-localized states.

a possible magnetic field asymmetry, which is not within the scope of our network model in the present state of development. Nevertheless, it is also possible to describe selective current injection into edge stripes within our network model, as e.g. achieved by selective EC reflection due to gate electrodes [85]. We cannot see how this could be achieved within the bulk current picture. Another important aspect to be mentioned at this point is that in our network the phase coherence is not maintained between the different grid periods, but still exact quantization of the QHE is obtained. This is in agreement with theoretical results of Gagel *et al* [55] who found a surprising stability of the QH plateaus against dissipation and phase destroying events.

Now we want to discuss our network model in view of the localization model introduced at the beginning of section 2. It is based on the idea that the total density of states of the LLs is divided into a fraction of de-localized states in an energy interval ΔE close to the centre of the LL and localized states outside in the tails of the LLs. Since our model does not address the localization problem explicitly, but addresses directly the transport properties instead, we want to look for the typical transport properties of a homogeneous regular QH sample as described by our model. For describing just the typical trends we can use an analytical formula instead of the network representation. This was already done in [68, 71] and we have shown that the total conductance G_{xx} of a QH sample is identical to the conductance of the partly filled top LL:

$$G_{xx} = \frac{e^2}{h}\frac{P}{1+P^2}. \tag{52}$$

With help of equations (43) and (52) we can plot G_{xx} with respect to the position of the Fermi energy E_{F} relative to the centre of the LL. In figure 27 we plot the density of states (DOS) versus Fermi energy E_{F} together with G_{xx} normalized to each other. The width of the DOS peak results from the overall LL broadening of the real sample, while the pre-factors in the exponent of equation (43) result from an idealized periodic 2D cosine potential modulation as derived in section 3. Without a randomization, this idealized periodic potential would be at the same time also responsible for the LL broadening, as used in the derivation of $P(\Delta\nu)$. However, it is quite clear that due to the randomization of the real potential landscape the overall broadening will be larger than that one suggested by the idealized periodic potential modulation. Since we can use directly equation (43) for calculating P, there is no need to associate the parameters in the exponent of equation (43) with a full periodic cosine potential. Instead, we can associate these parameters with the Taylor coefficients of the saddle potential at the tunnelling junction of a real potential. This is qualitatively shown in figure 28. Using the Taylor coefficients of

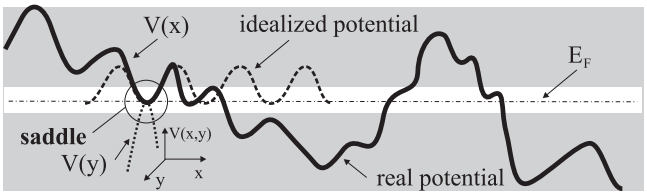

Figure 28. Schematic representation of the one-dimensional x-profile of a real fluctuating potential in comparison with the idealized potential used in section 3 in order to get the right Taylor coefficients for representing the encircled saddle. The white region around the saddle energy corresponds to the white region around the LL centre in figure 27.

the encircled saddle in figure 28 as the basis for an idealized two-dimensional cosine potential, the dashed cosine function, which matches the saddle curvature, would result. Consequently, the complete DOS broadening will be substantially larger than that one indicated by the Taylor coefficients of the saddles. However, the total DOS is responsible for the pinning behaviour of the Fermi level, while the Taylor coefficients of the saddle potential are responsible for the transport properties such as G_{xx}. As shown in figure 28, the Fermi level is assumed to come close to the saddle energy, which is marked by the circle. Using equation (43) for the tunnelling process is equivalent to assuming a two-dimensional cosine potential as indicated by the dashed plotted idealized potential. It is clear that not all saddles of the real potential come close to the Fermi energy and most of them are therefore physically inactive. Only by sweeping the magnetic field may different saddles become active and others inactive, just by the movement of the Fermi level relative to the potential landscape. If we consider such a saddle with an energy close to the centre of the broadened LL, it is clear that the parameters of equation (43) will not represent the real broadening of the LL. We can associate the whole pre-factor in the exponent of equation (43) with an energy interval, in which the Fermi energy will achieve a tunnelling current and, hence, at which the particular saddle can contribute to a de-localized state. As a consequence, if we plot G_{xx} as a function of E_{F}, we have to use the parameters of the saddle, which is associated with a small energy interval, while the plot of the DOS incorporates the full random potential. Reconsidering figure 27 one realizes a striking analogy with the localization–de-localization picture sketched in figure 1. This is also indicated by the two vertical lines representing the boundaries between localized and de-localized states in figure 27. This means that our model suggests qualitatively the same, although not relying directly on the localization model of the QHE, as e.g. achieved by the CC model. However, our model suggests that there could be a mixture of localized and de-localized states, where the weighting depends on the position of the Fermi level.

Considering our network representation, it appears as a regular network, while against the background of the above discussion a random network would be required instead of a regular network. However, as will be demonstrated in the following, our network model can also be understood as a theoretical concept for effective discretization of a random network. Obviously, lateral long range potential fluctuations will lead to a corresponding lateral fluctuation of the local filling factor, which, in turn, will lead to a lateral variation of the coupling function P of the nodes in our network. Suppose we wish to model a random potential on the basis of our regular network, then we need to choose the grid period to be much less than the typical length scale of the potential fluctuations. This is qualitatively shown in figure 29. The system is supposed to be close to half filling, which means the possibility of bulk current flow. However, half filling means $\overline{\nu} = 0.5$ on average and, due to the potential fluctuations, there will exist regions with locally $\nu > 0.5$ and regions with locally $\nu < 0.5$. In figure 29 the coloured

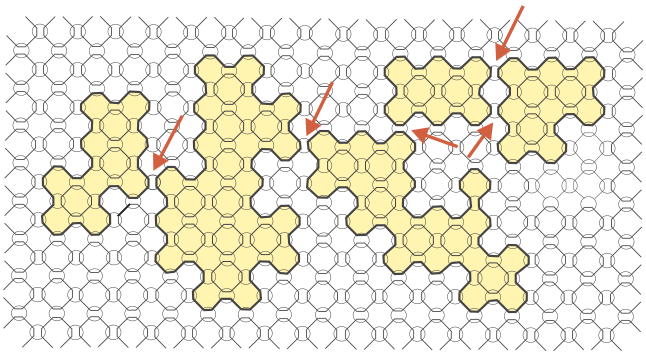

Figure 29. Cut-out of the bulk region showing the scheme of discretization of a random potential on the basis of our network model. The average filling factor of the associated Landau level is assumed to be close to $\nu = 0.5$. The coloured regions represent $\nu > 0.5$, which corresponds to a value of the coupling function $P \ll 1$ and the white regions represent $\nu < 0.5$, which corresponds to $P \gg 1$. The basic grid consists of alternating rows and lines of nodes in same orientation. Therefore, a change from $P \ll 1$ to $P \gg 1$ appears graphically as a rotation of the nodes by 90° within a line and a row, and as can be seen in the figure the corresponding nodes inside and outside the coloured area appear rotated against each other. Following now the inter-connections in the network, one can see that in this way a channel at the boundary between $\nu > 0.5$ and $\nu < 0.5$ is automatically guided to follow these boundaries (bold line). In real samples, this corresponds to a arbitrarily shaped magnetic bound state following the contour lines of the random potential. Most of the nodes with $P \ll 1$ or $P \gg 1$ serve as some sort of switching device in the network and are therefore not physically active. Only those near the saddle of the real potential, where also the real magnetic bound states get close together (marked by the red arrows), act physically as tunnelling junctions within the framework of the Landauer–Büttiker formalism.

regions represent $\nu > 0.5$ and the non-coloured regions $\nu < 0.5$. Most effective coupling at the nodes appears at $P = 1$, which corresponds to exact half filling $\nu = 0.5$. Due to the randomization of the potential, only a few of all nodes will remain close to half filling and most of them will depart from half filling, which leads to a coupling function of $P \ll 1$ in the coloured regions and $P \gg 1$ outside. However, $P \ll 1$ or $P \gg 1$ means mainly that an incoming channel is almost completely transmitted either to the one or the other outgoing channel of the node, which appears as a rotation of a node by 90° upon changing from one case to the other. As can be seen in figure 29 in this way our network guides the transmitted channels all around the boundaries between $\nu > 0.5$ and $\nu < 0.5$. Therefore, in this case, most of the nodes are physically inactive, but just switching the whole transmitted channel to either the one or the other outgoing channel. Only the nodes near the saddles of the real potential, where $\nu \approx 0.5$, and where also the real loops of the magnetic bound states get close to each other, become physically active by coupling different real loops. On this basis, our network can also be understood as an effective theoretical concept for setting up a random network with a discretization on a regular grid. However, already from considering figure 29, it is clear that a sufficient randomization of all conductor elements of a realistically shaped macroscopic sample geometry will require an increase in the size of the network by at least one order of magnitude in both directions in comparison to the simulations without randomization. For this reason, at present, a 'random network' modelling of a macroscopic Hall bar geometry is beyond our computing hardware capability. We tested the effect of randomization for a simple Hall bar geometry and found that the qualitative transport behaviour and all observed trends remain the same. Only a certain amount of additional broadening appeared on the plateau transitions and the R_{xx} peaks. Indeed, only details of the curvature, specially in the

tails of the R_{xx} peaks, appear sensitive to the details of the random potential. This is not surprising, however, since in a random potential, bulk current can be expected to become highly inhomogeneous near the percolation threshold. As we have aimed only to reproduce the main trends observed in magneto-transport studies in figures 20 and 21 or the 'anti-Hall-bar within Hall-bar geometry' in [113], we performed our calculations without randomization, and expect the main conclusions drawn from the simulations to hold their validity.

We have discussed already a number of aspects which support the argument that our network is well suited to account for the injection of non-equilibrium currents, which at the same time makes our network substantially different from the CC model. This is further supported by the fact that our simulation results agree perfectly with simulation results on the basis of a lattice model for the case of strong inelastic scattering [119]. In this lattice model inelastic scattering has to be artificially introduced by coupled virtual reservoirs in order to allow for dissipation. A possible presence of dissipation is already included in the formal description of the nodes in our network and the apparent disadvantage of having no phase coherence between different network periods turns out to be an advantage in this context. In contrast, the CC model has no possibility to handle dissipation, and therefore we cannot see how it could be turned into a circuit type model for simulating the distribution of experimentally excited currents and voltages.

6. Summary

We have introduced a circuit type network model for simulating the distribution of excited currents and voltages for magneto-transport experiments and compared it to different types of models for magneto-transport. We have shown that the possibility of dissipation is already included in the theoretical description of the nodes of our model. Although our network does not consider coherence between different network periods, it cannot be substituted by its classical counterpart of a simple resistor network. The main advantage of our network as compared to the Chalker–Coddington (CC) network is the fact that besides the ability to represent dissipative transport within the bulk, our network is also able to represent dissipationless transport even without considering full coherence, while in turn the coherent CC network does not account for dissipation. Starting with a treatment of the saddle-point problem in the high magnetic field limit by Büttiker, we have been able to show that it is possible to transform Büttiker's results into a filling-factor-dependent backscattering function $P(\Delta\nu)$. This function is used as the coupling function for the nodes of our network model for the QHE regime of 2D systems. As a result, the numerical simulations based on this network deliver transport data in which R_{xy} starts with a classical straight line while R_{xx} shows no zeros. With increasing magnetic field the IQHE sets in with Shubnikov–de Haas oscillations in R_{xx}, followed by zeros in R_{xx} and plateaus in R_{xy}, like seen in experimental data. For equilibrium conditions we have found an equivalence between the bulk current picture in terms of mixed phases as used by Ruzin *et al* and our network representation on the basis of the Landauer–Büttiker formalism. We have been able to show that an analogous interpretation to the localization–de-localization picture is also possible on the basis of our network model. In this context our model suggests a mixture between localized and de-localized states near the centre of the LL with a smooth transition from dominating de-localized to dominating localized states while the Fermi level moves away from the LL centre. Finally we have demonstrated that on the basis of our model a random potential situation can be represented. We argued that our network model is more closely related to a theoretical approach in terms of a lattice model for strong inelastic scattering as used by Ando *et al* than being related to the CC model. This makes our network model useable as some sort of circuit type network for modelling experimentally excited non-

equilibrium currents and voltages. The key point is that in our model phase coherence between different network periods is not explicitly requested, in contrast to the CC model, which in our opinion therefore cannot be used as a circuit type network for simulating experimentally injected non-equilibrium currents.

Acknowledgment

The authors thank M Büttiker for stimulating discussions and comments.

References

[1] Büttiker M 1988 *Phys. Rev.* B **38** 9375
[2] Chlovskii D B, Shklovskii B I and Glatzman L I 1992 *Phys. Rev.* B **46** 4026
[3] Hirai H and Komiyama S 1995 *Japan. J. Appl. Phys.* **34** 4321
[4] Christen T and Büttiker M 1996 *Phys. Rev.* B **53** 2064
[5] Wei H P, Tsui D C, Paalanen M A and Pruisken A M M 1988 *Phys. Rev. Lett.* **61** 1294
[6] Koch S, Haug R J, Klitzing K v and Ploog K 1991 *Phys. Rev. Lett.* **67** 883
[7] Koch S, Haug R J, Klitziung K v and Ploog K 1992 *Phys. Rev.* B **46** 1596
[8] Wei H P, Engel L W and Tsui D C 1994 *Phys. Rev.* B **50** 14609
[9] Hohls F, Zeitler U, Haug R J, Meisels R, Dybko K and Kuchar F 2002 *Phys. Rev. Lett.* **89** 2768011
[10] Huckestein B 1995 *Rev. Mod. Phys.* **67** 357
[11] Sondhy S L, Girvin S M, Carini J P and Shahar D 1997 *Rev. Mod. Phys.* **69** 315
[12] Ruzin I and Feng S 1995 *Phys. Rev. Lett.* **74** 154
[13] Klitzing K v, Dorda G and Pepper M 1980 *Phys. Rev. Lett.* **45** 494
[14] Fang F F and Stiles P J 1983 *Phys. Rev.* B **27** 6497
[15] Fang F F and Stiles P J 1984 *Phys. Rev.* B **29** 3749
[16] Streda P, Kucera J and MacDonald A H 1987 *Phys. Rev. Lett.* **59** 1973
[17] Jain J K and Kivelson S A 1988 *Phys. Rev. Lett.* **60** 1542
[18] Kane B E, Tsui D C and Weimann G 1987 *Phys. Rev. Lett.* **59** 1353
[19] Fertig H A and Halperin B I 1987 *Phys. Rev.* B **36** 7969
[20] van Wees B J *et al* 1988 *Phys. Rev. Lett.* **60** 848
[21] Wharam A *et al* 1988 *J. Phys. C: Solid State Phys.* **21** L209
[22] Komiyama S, Hirai H, Sasa S and Hiyamizu S 1989 *Phys. Rev.* B **40** 12566
[23] van Wees B J, Willems E M M, Harmans C J P M, Beenakker C W J, van Houten H, Williamson J G, Foxon C T and Harris J J 1989 *Phys. Rev. Lett.* **62** 1181
[24] van Wees B J, Kouvenhoven L P, Harmans C J P M, Williamson J G, Timmering C E, Broekaart M E I, Foxon C T and Harris J J 1989 *Phys. Rev. Lett.* **62** 2523
[25] Haug R J, Kucera J, Streda P and von Klitzing K 1989 *Phys. Rev.* B **39** 10892
[26] Alphenaar B W, McEuen P L, Wheeler R G and Sacks R N 1990 *Phys. Rev. Lett.* **64** 677
[27] Martin T and Feng S 1990 *Phys. Rev. Lett.* **64** 1971
[28] Müller G, Weiss D, Koch S, Klitzing K v, Nickel H, Schlapp W and Lösch R 1990 *Phys. Rev.* B **42** 7633
[29] Geim A K, Main P C, Beton P H, Streda P, Eaves L, Wilkinson C D W and Beaumont S P 1991 *Phys. Rev. Lett.* **67** 3014
[30] Simmons J A, Hwang S W, Tsui D C, Wei H P, Engel L W and Shayegan M 1991 *Phys. Rev.* B **44** 12933
[31] Ford C J B, Washburn S, Newbury R, Knoedler C M and Hong J M 1991 *Phys. Rev.* B **43** 7339
[32] van Son P C, de Vries F W and Klapwijk T M 1991 *Phys. Rev.* B **43** 6764
[33] Nii H, Ohsawa M, Komiyama S, Fukatsu S, Shiraki Y, Itoh R and Toyoshima H 1992 *Surf. Sci.* **263** 275
[34] Komiyama S, Hirai H, Ohsawa M, Matsuda Y, Sasa S and Fujii T 1992 *Phys. Rev.* B **45** 11085
[35] Alphenaar B W, Staring A A M, van Houten H, Mabesoone M A A and Foxon C T 1992 *Phys. Rev.* B **46** 7236
[36] Komiyama S, Hirai H, Ohsawa M, Matsuda Y, Sasa S and Fujii T 1992 *Phys. Rev.* B **45** 11085
[37] Merz R, Keilmann F, Haug R J and Ploog K 1993 *Phys. Rev. Lett.* **70** 651
[38] Maslov D L and Loss D 1993 *Phys. Rev. Lett.* **71** 4222
[39] Lee D H, Wang Z and Kivelson S 1993 *Phys. Rev. Lett.* **26** 4130
[40] Müller J E 1994 *Phys. Rev. Lett.* **72** 2616
[41] Main P C, Geim A K, Carmona H A, Brown C V, Foster T J, Taboryski R and Lindelof P E 1994 *Phys. Rev.* B **50** 4450

[42] Hirai H and Komiyama S 1994 *Phys. Rev.* B **49** 14012
[43] Peck A J, Bending S J, Weis J, Haug R J, Klitzing K v and Ploog K 1995 *Phys. Rev.* B **51** 4711
[44] Oto K, Takaoka S and Murase K 1995 *Japan. J. Appl. Phys.* **34** 4332
[45] Schuster R, Ensslin K, Dolgopolov V and Kotthaus J P 1995 *Phys. Rev.* B **52** 14699
[46] Kristensen A, Kennedy C J, Lindelof P E and Persson M 1995 *Semicond. Sci. Technol.* **10** 1315
[47] van Wees B J, Meijer G I, Kuipers J J, Klapwijk T M, van de Graaf W and Borghs G 1995 *Phys. Rev.* B **51** 7973
[48] van Haren R J F, de Lange W, Blom F A P and Wolter J H 1995 *Phys. Rev.* B **52** 5760
[49] Zozulenko I V, Maao F A and Hauge E H 1995 *Phys. Rev.* B **51** 7058
[50] Johnson B L, Sachrajda A S, Kirzenow G, Feng Y, Taylor R P, Henning L, Wang J, Zawadzki P and Colderidje P T 1995 *Phys. Rev.* B **51** 7650
[51] Mashida T, Hirai H, Komiyama S and Shiraki Y 1996 *Phys. Rev.* B **54** 16860
[52] Yahel E, Orgad D, Palevski A and Shtrikman H 1996 *Phys. Rev. Lett.* **76** 2149
[53] Rahman M, Davies J H, Larkin I A, Holland M C, Long A R and Williamson J G 1996 *Phys. Rev.* B **54** 16409
[54] Mani R G 1996 *J. Phys. Soc. Japan* **65** 1751
[55] Gagel F and Maschke K 1996 *Phys. Rev.* B **54** 13885
[56] Oswald J, Heigl G, Pippan M, Span G, Stellberger T, Maude D K and Portal J C 1996 *Surf. Sci.* **361/362** 525
[57] Oswald J, Heigl G, Span G, Homer A, Ganitzer P, Maude D K and Portal J C 1996 *Physica* B **227** 360
[58] Kao Y-C and Lee D-H 1996 *Phys. Rev.* B **54** 16903
[59] Mashida T, Hirai H and Komiyama S 1997 *Solid State Commun.* **103** 441
[60] Oswald J and Span G 1997 *Semicond. Sci. Technol.* **12** 345
[61] Bird J P, Stopa M, Connolly K, Pivin D P Jr, Ferry D K, Aoyagi Y and Sugano T 1997 *Phys. Rev.* B **56** 7477
[62] Shahar D, Tsui D C, Shayegan M, Shimshoni E and Sondhi S L 1997 *Phys. Rev. Lett.* **79** 479
[63] Tsemekhman K, Tsemekhman V, Wexler C and Thouless D J 1997 *Solid State Commun.* **101** 549
[64] Mani R G 1997 *Appl. Phys. Lett.* **70** 2879
[65] Oswald J, Heigl G, Span G, Homer A, Ganitzer P, Maude D K and Portal J C 1997 *Proc. 12th Int. Conf. on the Appl. of High Magnetic Fields (Würzburg, 1996)* vol 1 (Singapore: World Scientific) p 227
[66] Oswald J, Span G, Homer A, Heigl G, Ganitzer P, Maude D K and Portal J C 1997 *Solid State Commun.* **102** 391
[67] Shahar D *et al* 1997 *Solid State Commun.* **102** 817
[68] Oswald J, Span G and Kuchar F 1998 *Phys. Rev.* B **58** 15401
[69] Mashida T, Hirai H, Komiyama S and Shiraki Y 1998 *Physica* B **249–251** 128
[70] Furusaki A 1998 *Physica* B **249–251** 430
[71] Oswald J 1998 *Physica* E **3** 30
[72] Mashida T, Hirai H, Komiyama S and Shiraki Y 1998 *Solid-State Electron.* **42** 1155
[73] Oswald J, Span G, Homer A, Heigl G, Ganitzer P, Maude D K and Portal J C 1998 *Proc. 8th Int. Conf. on Narrow Gap Semiconductors (Shanghai, 1997)* (Singapore: World Scientific) pp 304–7
[74] Oswald J, Span G, Homer A, Heigl G, Ganitzer P, Maude D K and Portal J C 1998 *Proc. 8th Int. Conf. on Narrow Gap Semiconductors (Shanghai, 1997)* (Singapore: World Scientific) pp 300–3
[75] Ganitzer P, Homer A, Lucyshyn M, Jamnig B, Oswald J, Maude D K and Portal J C 1998 *Physica* B **256–258** 600–3
[76] Homer A, Ganitzer P, Span G and Oswald J 1999 *Superlatt. Microstruct.* **25** 191
[77] Oswald J, Homer A and Ganitzer P 1999 *Microelectron. Eng.* **47** 31
[78] Heinzel T, Acremann Y, Ensslin K, Gini E, Melchior H and Holland M 2000 *Physica* E **7** 804
[79] Mashida T, Ishizuka S, Muraki K, Hirayama Y and Komiyama S 2000 *Physica* E **6** 152
[80] Woodside M T, Vale C, McEuen P L, Kadow C, Maranowski K D and Gossard A C 2001 *Phys. Rev.* B **64** 041310/1
[81] Fujioka H, Katsumoto S and Iye Y 2001 *Japan. J. Appl. Phys.* **40** 2073
[82] Arai K, Oto K, Takaoka S and Murase K 2001 *Physica* E **9** 243
[83] Ahlswede E, Weitz P, Weis J, von-Klitzing K and Eberl K 2001 *Physica* B **298** 562
[84] Mashida T, Ishizuka S, Komiyama S, Muraki K and Hirayama Y 2001 *Phys. Rev.* B **63** 045318
[85] Oswald J and Homer A 2001 *Physica* E **11** 310
[86] Oswald J 2001 *Proc. 25th Int. Conf. on the Physics of Semiconductors (Osaka, 2000)* (*Springer Proceedings in Physics* vol 87) (Berlin: Springer) p 977
[87] Machida T, Ishizuka S, Yamazaki T, Komiyama S, Muraki K and Hirayama Y 2002 *Phys. Rev.* B **65** 233304
[88] Ahlswede E, Weis J, von-Klitzing K and Eberl K 2002 *Physica* E **12** 165
[89] Wurtz A, Wildfeuer R, Lorke A, Deviatov E V and Dolgopolov V T 2002 *Phys. Rev.* B **65** 075303
[90] Oswald J 2002 *SEMIMAG 15th Int. Conf. on High Magnetic Fields in Semiconductor Physics (Oxford, Aug. 2002)* CD-ROM

[91] Oswald J, Ochiai Y, Aoki N, Lin L-H, Ishibashi K, Aoyagi Y, Bird J P and Ferry D K 2002 *Microelectron. Eng.* **63** 91
[92] Aoki N, Lin L-H, Ochiai Y, Ishibashi K, Aoyagi Y, Bird J P, Ferry D K and Oswald J 2002 *Physica* E **13** 769
[93] Ensslin K 2003 *Superlatt. Microstruct.* **33** 425
[94] Komiyama S, Astafiev O and Machida T 2003 *Physica* E **20** 43
[95] Kawano Y and Komiyama S 2003 *Phys. Rev.* B **68** 085328
[96] Blaauboer M 2003 *Phys. Rev.* B **68** 205316
[97] Takashina K, Nicholas R J, Kardynal B, Mason N J, Maude D K and Portal J C 2003 *Phys. Rev.* B **68** 235303
[98] Büttiker M, Samuelsson P and Sukhorukov E V 2003 *Physica* E **20** 33
[99] Peled E, Shahar D, Chen Y, Diez E, Sivco D L and Cho A Y 2003 *Phys. Rev. Lett.* **91** 236802
[100] Machida T, Yamazaki T, Ikushima K and Komiyama S 2003 *Appl. Phys. Lett.* **82** 409
[101] Kawano Y and Komiyama S 2003 *Phys. Rev.* B **68** 085328
[102] Arai K, Hashimoto S, Oto K and Murase K 2003 *Phys. Rev.* B **68** 165347
[103] Cresti A, Grosso G and Parravicini G P 2004 *Phys. Rev.* B **69** 233313
[104] Sanchez D and Büttiker M 2004 *Phys. Rev. Lett.* **93** 106802
[105] Samuelsson P, Sukhorukov E V and Büttiker M 2004 *Phys. Rev. Lett.* **92** 026805
[106] Peled E, Chen Y, Diez E, Tsui D C, Shahar D, Sivco D L and Cho A Y 2004 *Phys. Rev.* B **69** 241305(R)
[107] Hehl F W, Obukhov Y N and Rosenow B 2004 *Phys. Rev. Lett.* **93** 096804
[108] Deviatov E V, Wurtz A, Lorke A, Melnikov M Yu, Dolgopolov V T, Reuter D and Wieck A D 2004 *Phys. Rev.* B **69** 115330
[109] Russ M, Lorke A, Reuter D and Schafmeister P 2004 *Physica* E **22** 506
[110] Seo Y, Eom B, Yu I, Park K and Lee S 2004 *Solid State Commun.* **130** 391
[111] Kicin S, Pioda T, Ihn T, Ensslin K, Driscoll D D and Gossard A C 2004 *Physica* E **21** 708
[112] Oswald M and Oswald J 2004 *J. Mod. Phys.* B **18** 27
[113] Oswald M, Oswald J and Mani R G 2005 *Phys. Rev.* B **72** 035334
[114] Landauer R 1957 *IBM J. Res. Dev.* **1** 223
[115] Büttiker M, Imry Y, Landauer R and Pinhas S 1985 *Phys. Rev.* B **31** 6207
[116] Halperin B I 1982 *Phys. Rev.* B **25** 2185
[117] Chalker J T and Coddington P D 1988 *J. Phys. C: Solid State Phys.* **21** 2665
[118] Ando T 1994 *Phys. Rev.* B **49** 4679
[119] Ando T 1998 *Surf. Sci.* **361/362** 270
[120] Cho S and Fisher M P A 1997 *Phys. Rev.* B **55** 1637
[121] Arovas D P, Janssen M and Shapiro B 1997 *Phys. Rev.* B **56** 4751
[122] Cain P, Römer R A, Schreiber M and Raikh M E 2001 *Phys. Rev.* B **64** 235326
[123] Kramer B, Ohtsuki T and Kettemann S 2006 *Phys. Rep.* **417** 211–342
(Kramer B, Ohtsuki T and Kettemann S 2004 *Preprint* cond-mat/0409625)
[124] Hohls F, Zeitler U and Haug R J 2002 *Phys. Rev. Lett.* **88** 036802
[125] Ando T and Aoki H 1985 *J. Phys. Soc. Japan* **54** 2238
[126] Büttiker M 1985 *Phys. Rev.* B **32** 1846
[127] Büttiker M 1986 *Phys. Rev.* B **33** 3020
[128] D'Amato J L and Pastawski H M 1990 *Phys. Rev.* B **41** 7411
[129] Büttiker M 1990 *Phys. Rev.* B **41** 7906